

Binary Survival in the Outer Solar System

David Nesvorný¹, David Vokrouhlický²

(1) *Department of Space Studies, Southwest Research Institute,
1050 Walnut St., Suite 300, Boulder, CO, 80302, USA*

(2) *Institute of Astronomy, Charles University,
V Holešovičkách 2, CZ-18000 Prague 8, Czech Republic*

ABSTRACT

As indicated by their special characteristics, the cold classical Kuiper belt objects (KBOs) formed and survived at $\simeq 42\text{--}47$ au. Notably, they show a large fraction of equal-size binaries whose formation is probably related to the accretion of KBOs themselves. These binaries are uncommon in other –hot, resonant, scattered– populations, which are thought to have been implanted from the massive disk below 30 au to >30 au during Neptune’s migration. Here we highlight the possibility that equal-size binaries formed in the disk but were subsequently removed by impacts and/or dynamical effects (e.g., scattering encounters with Neptune). We determine the dependence of these processes on the size and separation of binary components. Our results indicate that tighter binaries, if they formed in the massive disk, have relatively good chances of survival (unless the disk was long-lived). In contrast, the widest binaries in the hot population, such as 2002 VF130, have a very low survival probability ($<1\%$) even if the massive disk was short-lived. They may represent a trace of lucky survivors of a much larger population of the original disk binaries, or they formed at $\sim 30\text{--}40$ au and dodged the impact- and encounter-related perturbations that we studied here. We find that all known satellites of the largest KBOs would survive during the dynamical implantation of these bodies in the Kuiper belt. The low orbital eccentricities of Pluto’s small moons may have been excited by impacts and/or encounters of the Pluto system to Neptune.

Subject headings:

1. Introduction

The Kuiper belt is a population of icy bodies beyond the orbit of Neptune (Figure 1). The orbital structure of the Kuiper belt is an important constraint on the early evolution of

the Solar System. It is thought that much of this structure, with large resonant populations and dynamically excited orbits, has emerged as a result of Neptune’s migration into an outer disk of planetesimals (e.g., Hahn & Malhotra 2005, Levison et al. 2008). The massive planetesimal disk that presumably existed below 30 au was completely dispersed by Neptune, and a small fraction of the scattered population was implanted onto orbits beyond 30 au, where it overlaps in orbital space with a population of bodies that formed and survived at >30 au (e.g., Batygin et al. 2011). Here we study an important tracer of this process, the KBO *binarity*, to set constraints on the initial binary fraction, planetesimal disk lifetime and timing of planetary migration.

Observations provide direct evidence for two different populations in the Kuiper belt. On one hand, Plutinos in the 3:2 resonance with Neptune, other resonant populations, Hot Classical (HCs) and Scattered Disk Objects (SDOs; see Gladman et al. 2008 for a definition of these categories) share similar physical attributes. These populations (hereafter the dynamically *hot* KBOs) are thought to have been implanted into the Kuiper belt from below 30 au. The Cold Classical (CCs), on the other hand, have low orbital inclinations (Brown 2001, Gulbis et al. 2010), distinctly red colors (Tegler & Romanishin 2000), relatively high albedo (Brucker et al. 2009, Vilenius et al. 2014), and a size distribution that shows a very steep slope at large sizes (Bernstein et al. 2004). The CCs are believed to have formed at $\simeq 42\text{-}47$ au where they are found now.

Another important difference between the dynamically hot and cold populations in the Kuiper belt is the existence and nature of *binary* objects. A very large fraction of known 100-km-class CCs are resolved binaries with nearly equal-size components (Noll et al. 2008a,b, Fraser et al. 2017, Grundy et al. 2018). These binaries are thought to have formed during the formation of KBOs themselves or by early capture (e.g., Goldreich et al. 2002, Nesvorný et al. 2010). Many CC binaries have widely separated components which can become unbound as a result of small collisions (Petit & Mousis 2004). In contrast, the equal-size binaries are nearly absent in the hot population. Instead, in the hot population, it is more common to have a small satellite orbiting a much larger primary. These moons are thought to have accreted around primaries from impact-generated disks (Canup 2005, Leinhardt et al. 2010).

The most straightforward interpretation of these differences is that collisions played an important role in shaping the hot population, whereas the collisional evolution of CCs

was relatively modest (Nesvorný et al. 2011, Parker & Kavelaars 2012). The collisional activity in the present Kuiper belt is low and not very different between the hot and cold populations. This means that the hot population must have collisionally evolved *before* it was implanted into the Kuiper belt, probably during a stage when it was embedded in the massive planetesimal disk. CCs did not follow the same evolution path most likely because the outer extension of the planetesimal disk at >40 au had a relatively low mass. In addition, it has been pointed out (Parker & Kavelaars 2010) that the wide binaries in the CC population would not dynamically survive during the implantation process, thus strengthening the idea that they formed beyond $\simeq 40$ au.

The goal of this work is to establish the survival rate of binaries that formed in the massive planetesimal disk below 30 au.¹ First, before their implantation into the Kuiper belt, binaries can become unbound by kicks induced by small impacts. Second, during their implantation in the Kuiper belt, binaries have close encounters with migrating Neptune. Wide binaries can become unbound if Neptune’s tidal potential during an encounter exceeds the binary binding energy (Parker & Kavelaars 2010). More tightly bound binaries may have survived because their binding energy is greater. In addition, impacts and dynamical perturbations can change binary orbits, leading in some cases to a low-speed collision between binary components (Nesvorný et al. 2018). This could potentially represent an interesting channel for the formation of *contact* binaries (e.g., Sheppard & Jewitt 2004, Thirouin & Sheppard 2018).

Binary survival in the massive planetesimal disk depends on the disk’s lifetime, t_{disk} . Clearly, if the disk was short-lived ($t_{\text{disk}} < 100$ Myr), fewer collisions would have occurred, and binaries would have had a better chance of survival than in the case of a long-lived disk ($t_{\text{disk}} > 100$ Myr). The disk lifetime, in turn, is related to the timing of Neptune’s migration. In addition, the dynamical survival of binaries during their implantation into the Kuiper belt depends on the number and nature of planetary encounters, and ultimately on the orbital

¹A handful of equal-size binaries have been detected on highly inclined heliocentric orbits in the dynamically hot population (e.g., 2002 VF130, 2004 PB108; Section 3). Their existence indicates that the formation of equal-size binaries was widespread and also occurred in the massive disk below 30 au, which is thought to be the main source of the hot population. Indeed, the suggested binary formation mechanisms show only a weak dependence on the radial distance.

behavior of planets. We thus see that the binary occurrence in the Kuiper belt can be used, at least in principle, to constrain Neptune’s migration and the implantation process itself.

In summary, the goal of this paper is to test a specific hypothesis: that binaries in transneptunian populations other than low inclination CCs originally formed at lower heliocentric distance and were transported to their current orbits by way of interactions with giant planets. This hypothesis is currently the most frequently asserted and is consistent with several observed features of the population, but many uncertainties remain, for example, related to the radial profile of the planetesimal disk. Here we adopt an assumption that the source of the entire hot population was a massive planetesimal disk with an outer edge at ~ 30 au. This remains a hypothesis. We find that the existence of very wide binaries in the hot population may not be fully consistent with this hypothesis, possibly indicating that at least part of the hot population started beyond the reach of Neptune at >30 au.

2. Previous Work on Binary Survival

The problem of KBO binary survival was considered in several publications. Petit & Mousis (2004) pointed out that small impacts can dissolve a binary if the velocity change produced by impacts is comparable to binary’s orbital speed (typically meters per second for known KBO binaries). The work determined the expected lifetime of several binaries in the current Kuiper belt environment (and discussed the effects of primordial grinding as well). Using a reference size distribution of impactors with $N(R) \propto R^{-4.5}$ for radius $R > 5$ km and $N(R) \propto R^{-3}$ for $R < 5$ km, they found that wide binaries such as 1998 WW31 and 2001 QW322 have expected lifetimes of only ~ 1 -2 Gyr. This would suggest that these binaries have been much more common in the early Solar System (for a few to survive to the present day).

The effect of impacts, however, depends on the assumed size distribution of impactors and much longer lifetimes are inferred if $N(R) \propto R^{-3}$ for $5 < R < 50$ km, as suggested by modern observational surveys, Charon craters and other constraints (e.g., Bernstein et al. 2004, Morbidelli et al. 2009, Parker & Kavelaars 2012, Fraser et al. 2014, Nesvorný et al. 2018, Singer et al. 2019). Additional mechanisms studied in Petit & Mousis (2004), such as collisional disruption and gravitational scattering by large KBOs, were found to be less of

an issue for binary survival. Shannon & Dawson (2018) modeled the effect of gravitational scattering in detail and concluded that the existence of wide CC binaries is consistent with ~ 1000 -4000 Pluto-mass objects in the original disk (Nesvorný & Vokrouhlický 2016).

Nesvorný et al. (2011) extended the work of Petit & Mousis (2004) by modeling impacts in the early Solar System. They showed that the existence of CC binaries can be used to set limits on the extent of collisional grinding in the primordial Kuiper belt and suggested that the observed rollover of CCs with $R > 50$ km (e.g., Fraser et al. 2014) was probably not produced by disruptive collisions. Instead, it may be a fossil remnant of the KBO formation process. In contrast, the size distribution break at $R \sim 50$ km in the hot population was most likely produced by collisional grinding during the early stages (e.g., Nesvorný et al. 2018). Here we consider the effects of primordial grinding on binaries found in the hot population and show that some of them (e.g., 2002 VF130) are expected to have a very low survival probability. This has interesting implications for the initial binary fraction and/or for the original source reservoir of binaries now found in the hot population.

The *dynamical* survival of binaries found in the cold population was studied in Parker & Kavelaars (2010) and Fraser et al. (2017). Parker & Kavelaars (2010) showed that the large binary fraction in the cold population is inconsistent with them being implanted to $\simeq 42$ -47 au from a massive disk below ~ 35 au (Levison et al. 2008). This is because bodies starting below ~ 35 au often have scattering encounters with Neptune before reaching $\simeq 42$ -47 au, and most wide binaries are dissolved in the process. The binary constraint therefore gives a strong support to the idea that the CC population formed beyond ~ 35 au (see Section 5.1 for additional discussion of Parker & Kavelaars 2010). Fraser et al. (2017) complemented these results by demonstrating that some wide CC binaries (presumably the ones with less red colors) could have been pushed from ~ 38 -42 au to > 42 au by the 2:1 resonance with migrating Neptune.

Here we study the effects of planetary encounters on binaries starting in the massive disk below ~ 30 au and reaching orbits in the hot population (i.e., HCs, resonant and scattered objects). This scientific problem was not considered before (see Noll et al. 2006 and Nesvorný et al. 2018 for related studies of Centaurs and Jupiter Trojans) at least partly because we did not have a reliable model for the implantation of objects in the Kuiper belt. Here we use the implantation model of Nesvorný & Vokrouhlický (2016), which has a long heritage

in the previous works on the subject (e.g., Hahn & Malhotra 2005, Levison et al. 2008). The model of Nesvorný & Vokrouhlický (2016) with slow and grainy migration of Neptune was shown to match the observed orbital structure of the Kuiper belt (inclination distribution, ratio of resonant and non-resonant objects, etc). Some of the model predictions (Kaib & Sheppard 2016, Nesvorný et al. 2016) have already been confirmed from new observations (e.g., Lawler et al. 2019).

3. Known Kuiper Belt Binaries

A catalog of physical and orbital properties of binary bodies is maintained W. R. Johnston (Johnston 2018) on the NASA Planetary Data System (PDS) node.² We analyzed the PDS catalog in September 2018. Figure 2 shows the basic properties of KBO binaries/satellites. Several notable features are apparent in the plot. First, the unequal-size binaries with a large primary and a small moon ($R_2/R_1 < 0.5$, where R_1 and R_2 denote the primary and secondary radii) are mainly detected around large primaries in the hot population. They are absent in the cold population either because they did not form or because bodies in the CC population are generally smaller and the moons with $R_2 < 0.5 R_1$ around small primaries are difficult to detect. Second, most known equal-size binaries with $R_2/R_1 > 0.5$ appear in the cold population (40 out of 65 known; shown in red in Fig. 2).

Two (1998 WW31 and (119067) 2001 KP76) of only seven known HC binaries (see Section 4.1 for our definition of dynamical categories) with $R_2/R_1 > 0.5$ have the heliocentric inclinations slightly above our cutoff limit of 5° and may be interlopers from the CC population (Fraser et al. 2017). This applies to (341520) Mors-Somnus and (82157) 2001 FM185, both in the Plutino population, as well.³

Of the remaining five, 2002 VF130 has the largest binary separation ($a_B/R_B \simeq 310$, where a_B is the binary semimajor axis and $R_B^3 = R_1^3 + R_2^3$), and 2004 PB108 and 2004 KH19 have $a_B/R_B \simeq 81$ and 130, respectively (Table 1). These wide binaries in the HC population

²<https://sbn.psi.edu/pds/resource/binmp.html>

³(82157) 2001 FM185 with $a = 38.7$ au was classified as CC by the Deep Ecliptic Survey. Here we prefer to relate it to the 3:2 resonance ($a = 39.4$ au) and include it in the present analysis.

represent the most interesting constraint. All other nearly equal-size binaries in the HC population have $a_B/R_B \lesssim 30$ and better odds of survival (Section 5). In addition, (47171) Lempo (provisory designation 1999 TC36) is a triple system in the Plutino population with $R_3/R_1 \simeq 0.5$ and $a_B/R_B \simeq 50$, where R_3 is the radius of the tertiary component. The scattered disk binary 2006 SF369 has $R_2/R_1 \simeq 0.98$ and $a_B/R_B \simeq 35$.

4. Method

4.1. Dynamical Effect of Planetary Encounters

We make use of the simulations published in Nesvorný & Vokrouhlický (2016). See this work for the description of the integration method, planet migration, initial orbital distribution of disk planetesimals, and comparison of the results with the orbital structure of the Kuiper belt. A shared property of the selected runs is that Neptune migrates outward by scattering planetesimals (Table 2). Planetesimals were initially distributed in a disk extending from just beyond the initial orbit of Neptune at 22 au to 30 au. The outer extension of the disk beyond 30 au was ignored, because various constraints indicate that a large majority of planetesimals started at <30 au (e.g., Gomes et al. 2004). The simulations were performed with a modified version of the symplectic N -body integrator known as *Swift* (Levison & Duncan 1994).

All encounters of planetesimals with planets were recorded during these simulations. This was done by monitoring the distance of each planetesimal from Jupiter, Saturn, Uranus and Neptune, and recording every instance when the distance dropped below $0.5 R_{\text{Hill},j}$, where $R_{\text{Hill},j}$ are the Hill radii of planets ($j = 5$ to 8 from Jupiter to Neptune). We verified that the results do not change when more distant encounters are accounted for.

We selected disk planetesimals that ended up in different KBO populations at the end of simulations ($t = 4.5$ Gyr). Specifically, we defined the following four categories: HCs (semimajor axes $40 < a < 47$ au, perihelion distances $q > 36$ au, orbital inclinations $i > 5^\circ$), Plutinos (stable librations in the 3:2 resonance), scattering ($50 < a < 200$ au, >1.5 au change in a in the last Gyr; Gladman et al. 2008) and detached ($50 < a < 200$ au, <1.5 au change) objects. We used a longer time interval than Gladman et al. (2008) to distinguish

between the scattering and detached populations. Our definition of the detached population is therefore more restrictive. The CC population ($42 < a < 47$ au, $q > 36$ au, $i < 5^\circ$) was not considered here.⁴ Note that the distinction between CCs and HCs based on a single inclination cutoff is somewhat arbitrary.

Each selected planetesimal was assumed to be a binary object. We considered a range of binary separations ($1 < a_B/R_B < 2000$), initially circular orbits (binary orbit eccentricity $e_B = 0$), and a random distribution of binary inclinations (i_B). In some instances, several clones with different binary inclinations were assigned to each selected planetesimal to increase the statistics. Each binary was evolved through each recorded planetary encounter. We used the Bulirsch-Stoer (B-S) N -body integrator that we adapted from Numerical Recipes (Press et al. 1992). The center of mass of each binary planetesimal was first integrated backward from the time of the closest approach to $3 R_{\text{Hill}}$. It was then replaced by the actual binary and integrated forward through the encounter until the planetocentric distance of the binary exceeded $3 R_{\text{Hill}}$.⁵ The final binary orbit was used as an initial orbit for the next encounter and the algorithm was repeated over all encounters.

The B-S code monitored collisions between binary components. If a collision occurred, the integration was stopped and the impact speed and angle were recorded. A fraction of binaries became unbound. For the surviving binaries, we recorded the final values of a_B , e_B and i_B , which were then used to evaluate the overall change of orbits. After all integrations finished, we combined the individual runs into a statistical ensemble of possibilities. The results convey the dynamical survival probability of binaries in each KBO category.

4.2. Collisional Survival

The mutual orbit of a binary can be affected by small impacts into its components (Petit & Mousis 2004). Here we investigate this process with the collision code that we previously developed (Morbidelli et al. 2009, Nesvorný et al. 2011). The code, known as

⁴If the CC population formed at $a \simeq 40$ au, the CC binaries have not experienced planetary encounters (e.g., Fraser et al. 2017).

⁵The code is available upon request from authors.

Boulder, employs a statistical method to track the collisional fragmentation of planetesimal populations. It was developed along the lines of other published codes (e.g., Weidenschilling et al. 1997, Kenyon & Bromley 2001). A full description of the *Boulder* code, tests, and various applications can be found in Morbidelli et al. (2009), Levison et al. (2009) and Bottke et al. (2010). Here we briefly highlight the main points and differences with respect to these publications.

For each collision, the code computes the specific impact energy Q and the critical impact energy Q_D^* for catastrophic disruption (see Benz & Asphaug (1999) for definitions). Based on the value of Q/Q_D^* and available scaling laws, it then determines the masses of the largest remnant and largest fragment, and the power-law size distribution of smaller fragments (e.g., Durda et al. 2007). The Q_D^* function in *Boulder* was set to be intermediate between the impact simulations with strong (Benz & Asphaug 1999) and weak ice (Leinhardt & Stewart 2009). To achieve this, we multiplied Q_D^* from Benz & Asphaug (1999) by a factor f_Q , where $f_Q = 1, 0.3$ and 0.1 was used in different tests.

The main input parameters are: the (i) initial size distribution of simulated populations, (ii) intrinsic collision probability P_i , and (iii) mean impact speed v_i . As for P_i and v_i , we performed two different tests. The first test was intended to replicate the collisional grinding of the massive planetesimal disk. In this case, we assumed that migrating Neptune removed the disk at t_{disk} after the dispersal of the protosolar nebula (t_0), and let the disk collisionally evolve over t_{disk} . The dynamical state of the disk was taken from Levison et al. (2011). For example, at 300 Myr after t_0 , the disk at 20-30 au is characterized by $P_i \simeq 8 \times 10^{-21} \text{ km}^{-2} \text{ yr}^{-1}$ and $v_i \simeq 0.4 \text{ km s}^{-1}$ (Morbidelli & Rickman 2015).

The second set of tests with *Boulder* was done under the assumption that the outer planetesimal disk was dispersed by Neptune immediately after t_0 (i.e., $t_{\text{disk}} = 0$). The disk was assumed to have started dynamically cold ($e \simeq 0$ and $i \simeq 0$). It was gradually excited after t_0 , on a timescale of $\sim 10\text{-}30$ Myr (Table 2), by migrating Neptune. The Öpik algorithm (Wetherill 1967, Greenberg 1982) and the simulations reported in Nesvorný & Vokrouhlický (2016) were used to compute P_i and v_i as a function of time. We monitored the collision probabilities and impact velocities of the selected planetesimals (i.e., the ones that ended up in one of the considered KBO categories at $t = 4.5$ Gyr) with all other planetesimals. The P_i and v_i values were computed each δt by averaging over the selected planetesimals, where

$\delta t = 1$ Myr during the initial stages, when P_i and v_i change quickly, and $\delta t = 10\text{-}100$ Myr later on.

The initial size distribution of the massive disk can be informed from the planetesimal formation models (e.g., Simon et al. 2017), but we considered other possibilities as well (Section 5.3). The final size distribution was required to match the shape of the size distribution of Jupiter Trojans (see, e.g., Morbidelli et al. 2009, Nesvorný et al. 2013, Fraser et al. 2014, Singer et al. 2019 for a justification of this assumption), which is well characterized from observations down to at least 3 km diameter, D (Wong & Brown 2015, Yoshida & Terai 2017). For $5 \lesssim D \lesssim 100$ km, the cumulative size distribution $N(>D)$ is a power law $N(>D) \propto D^{-\gamma}$ with $\gamma \simeq 2.1$. Above $D \simeq 100$ km, the Jupiter Trojan size distribution bends to a much steeper slope ($\gamma \sim 6$).

To construct the size distribution of planetesimals in the massive disk, the Jupiter Trojan size distribution was divided by P_{JT} , where $P_{\text{JT}} = 5 \times 10^{-7}$ is the Jupiter Trojan capture probability determined in Nesvorný et al. (2013) (this is a probability that an outer disk planetesimal ends up on a stable Jupiter Trojan orbit). This gives $\simeq 6 \times 10^9$ disk planetesimals with $D > 10$ km or $\simeq 5 \times 10^7$ disk planetesimals with $D > 100$ km. The total mass of the reconstructed population is $\simeq 20 M_{\oplus}$, where M_{\oplus} is the Earth mass, in agreement with the results of Nesvorný & Morbidelli (2012).

4.3. Binary Module

The binary module in *Boulder* (Nesvorný et al. 2011) accounts for small, non-disruptive impacts on binary components, and computes the binary orbit change depending on the linear momentum of impactors. For each impact, the change of orbital speed, $\mathbf{v}_B = \mathbf{v}_2 - \mathbf{v}_1$, where \mathbf{v}_1 and \mathbf{v}_2 are the velocity vectors of components, is computed from the conservation of the linear momentum. This gives

$$\delta \mathbf{v}_B = \frac{m_i}{m_2 + m_i} \left(\frac{1}{2} \mathbf{v}_i - \frac{m_1}{m_B} \mathbf{v}_B \right) \quad (1)$$

for an impact on the secondary, and

$$\delta \mathbf{v}_B = -\frac{m_i}{m_1 + m_i} \left(\frac{1}{2} \mathbf{v}_i + \frac{m_2}{m_B} \mathbf{v}_B \right) \quad (2)$$

for an impact on the primary, where m_1 and m_2 are the primary and secondary masses, $m_B = m_1 + m_2$, and m_i and \mathbf{v}_i are the impactor’s mass and velocity.

The first term in Eqs. (1) and (2) corresponds to the transfer of the linear momentum. The factor 1/2 stands for the contribution of impactor’s linear momentum to the translational motion (as averaged over all impact geometries). The rest of linear momentum is consumed by the spin vector change of the impacted binary component. Note that this assumes that all collisions are completely inelastic.

The impact velocity vectors were assumed to be randomly oriented in the reference frames of binaries. We also factored in that impacts can happen at any orbital phase and averaged the binary orbit changes over the orientation and phase. The changes of orbital elements, δa_B and δe_B , were computed from

$$\frac{\delta a_B}{a_B} = \pm \frac{1}{\sqrt{3}} \frac{m_i v_i}{m_B v_B} \quad (3)$$

and

$$\delta e_B = \pm \frac{1}{2} \sqrt{\frac{5}{6}} \eta \frac{m_i v_i}{m_B v_B}, \quad (4)$$

where v_i and v_B are the moduli of \mathbf{v}_i and \mathbf{v}_B , and $\eta^2 = 1 - e_B^2$. The \pm sign in front of the right-hand sides indicates that the individual changes can be positive or negative. Equations (3) and (4) were implemented in the *Boulder* code. A similar expression can be obtained for inclinations (Nesvorný et al. 2011), but we do not discuss the inclination changes here.

5. Results

5.1. Dynamical Survival

We first evaluated the dynamical effect of planetary encounters. Using methods described in Section 4.1, we determined how the survival probability depends on the size and separation of binary components. We found that the binary survival depends on a_B/R_B , where $R_B = (R_1^3 + R_2^3)^{1/3}$, and not on a_B , R_1 and R_2 individually. This is a consequence of the binary dissociation condition described in Agnor & Hamilton (2006). A binary with the total mass $m_B = m_1 + m_2$ can become unbound when the planetocentric Hill radius of the binary, $r_{\text{Hill},B} = q(m_B/3m_{\text{pl}})^{1/3}$, where q is the distance of the closest approach and m_{pl}

is the planet mass, becomes smaller than the binary separation; that is $r_{\text{Hill,B}} < a_{\text{B}}$. This condition yields

$$\frac{a_{\text{B}}}{R_{\text{B}}} > \frac{1}{3^{1/3}} \left(\frac{\rho}{\rho_{\text{pl}}} \right)^{1/3} \left(\frac{q}{R_{\text{pl}}} \right), \quad (5)$$

where R_{pl} and ρ_{pl} are the planet radius and density. Here we assumed that the primary and secondary components of binaries have the same density, ρ . For exactly equal-size binaries with $R_1 = R_2$, $R_{\text{B}} = (R_1 + R_2)/2^{2/3}$.

The closest encounters with Neptune typically have $q/R_{\text{pl}} \sim 40$ in our simulations, suggesting that binaries with $a_{\text{B}}/R_{\text{B}} > 30$ should often become dissociated. This closely corresponds to Fig. 3, where the survival probability for $a_{\text{B}}/R_{\text{B}} > 30$ is $< 50\%$.

The survival probability is a strong function of binary separation (Figure 3). The binaries with small separations ($a_{\text{B}}/R_{\text{B}} < 30$) are tightly bound together and have high survival probabilities (50-90%). They are affected only during extremely close encounters to planets, which do not happen too often. The binaries with larger separations ($a_{\text{B}}/R_{\text{B}} > 30$) are more likely to become dissolved. This is expected because the wide binaries suffer larger orbital changes during planetary encounters. Also, in about 10% of cases, binaries end up their existence during a collision between the binary components (the N -body code stops when a collision is identified), which may have interesting implications for the origin of contact binaries in the Kuiper belt (Section 6.1).

The results shown in Figure 3 were computed assuming the bulk density $\rho = 1 \text{ g cm}^{-3}$. According to Eq. (5), the critical semimajor axis scales with $\rho^{1/3}$. Therefore, the surviving fraction curve shown in Figure 3 would shift left by a multiplication factor of 0.79 for $\rho = 0.5 \text{ g cm}^{-3}$ and right by a multiplication factor of 1.26 for $\rho = 2.0 \text{ g cm}^{-3}$. We confirmed this by simulating cases with different densities.

The dynamical survival probabilities shown in Figure 3 are lower than those reported in Parker & Kavelaars (2010). They found a $\simeq 60\%$ survival probability for $a_{\text{B}}/R_{\text{B}} = 200$, whereas we only find $\simeq 2.5\%$ probability. This is, in part, related to a much richer history of planetary encounters in our model with the slow migration of Neptune. Parker & Kavelaars (2010), instead, assumed a strong instability case from Levison et al. (2008). Additional differences arise due to different selection criteria. In Figure 3, we selected all bodies that ended in the HC population at $t = 4.5 \text{ Gyr}$. Parker & Kavelaars (2010) monitored each

particles semimajor axis and eccentricity for 1 Myr after the instability and identified all candidates that passed through “CC-like” orbits (which no longer have close encounters with Neptune). As explained in Levison et al. (2008), these candidates typically start with low orbital inclinations at $\simeq 30\text{--}34$ au and their inclinations remain low because they experience fewer-than-average scattering encounters with Neptune. This can readily explain the difference between our Figure 3 and Parker & Kavelaars (2010), because fewer and/or more distant encounters imply better chances of binary survival. The minimum encounter distance to Neptune reported in their Figure 1 is $q \simeq 0.1$ au, whereas we often have $q \simeq 0.01$ au.

For Plutinos, HCs and detached objects, all planetary encounters happen during the initial stages before objects are implanted onto stable orbits in the Kuiper belt. Only the scattered disk objects remain coupled to Neptune. For them, $>90\%$ of the recorded planetary encounters happen within the first $\simeq 200$ Myr of the simulation. This implies that binaries are typically removed early, or never, and the binary fraction in the scattering population does not change much in the last 4 Gyr (see Section 5.5 for a discussion of the Kozai resonance for binaries with $i_B \sim 90^\circ$; Porter & Grundy 2012).

Finally, we compare the results for different KBO populations (Figure 4) and for different migration histories of Neptune (Figure 5). Figure 4 shows that no significant differences are expected between different KBO populations. This is a consequence of the statistically similar histories of planetary encounters for bodies implanted into different populations. There are also no important differences between the two cases considered here with different timescales of Neptune’s migration (Figure 5). In case1 (Table 2), there are on average 12 (0.35) encounters within 0.1 au (0.01 au) to Neptune for each captured HC object. In case2, there are on average 10 (0.33) such encounters. The two cases are therefore expected to produce similar survival probabilities.

5.2. Orbits of Surviving Binaries

Planetary encounters act to change binary orbits. Figure 6 illustrates the relationship between the initial and final semimajor axes of the surviving binaries. The orbital changes are minimal for $a_B/R_B < 30$, but increase with binary separation. For example, 90% of surviving

orbits that end up with $a_B/R_B = 40$ start with $30 < a_B/R_B < 60$. For $a_B/R_B > 100$, the orbital changes are major and the binary semimajor axis can change by more than a factor of 2.

Figure 7a shows the distribution of final separations for binaries started with $a_B/R_B = 50$. Whereas most orbits remain with the semimajor axes near the original one, the distribution also shows wide wings toward lower and higher values. For example, $\simeq 10\%$ of surviving orbits end up with $a_B/R_B > 70$. This shows that at least some of the wide KBO binaries in the hot populations could have started with tighter orbits.

The binary eccentricity changes can be substantial as well (Figure 7b). For example, the mean eccentricity of the surviving orbits with initial $a_B/R_B = 50$ is $e_B \simeq 0.3$ (this assumes that $e_B = 0$ initially). Thus, even if the equal-size KBO binaries in the dynamically cold and hot population presumably formed by the same mechanism, and initially had the same distribution of binary orbits, they are not expected to be the same today.

5.3. Collisional Survival of Binaries in the Massive Disk

The collisional evolution of the massive outer disk was studied in Nesvorný et al. (2018). They showed that the Patroclus-Menoetius (P-M) binary in the Jupiter Trojan population poses an important constraint on the massive disk lifetime (t_{disk}). This is because the longer the P-M binary stays in the disk, the greater is the likelihood that its components will be stripped from each other (by the impact-related process described in Section 4.3; Petit & Mousis 2004). They found that the massive disk must have been dispersed by the migrating planets within ~ 100 Myr after the removal of the protosolar nebula (i.e., $t_{\text{disk}} \lesssim 100$ Myr). Here we first briefly recall their results related to the collisional grinding of the massive disk.

The collisional grinding of the outer planetesimal disk proceeds fast. For $t_{\text{disk}} > 100$ Myr, the number of $D > 10$ km bodies is reduced at least ten times and the total mass drops to $< 10 M_{\oplus}$. These results are in conflict with the current size distribution of Jupiter Trojans (Wong & Brown 2016), the planetesimal disk mass inferred from the Jupiter Trojan capture (Morbidelli et al. 2005, Nesvorný et al. 2013), and other constraints (e.g., Nesvorný & Morbidelli 2012). The problem could potentially be resolved if a larger initial mass was

adopted. Nesvorný et al. (2018) tested several possibilities along these lines. For example, they scaled up the reference size distribution by an additional factor to increase the initial mass to $>20 M_{\oplus}$. These tests failed because more massive disks grind faster and end up with $<10 M_{\oplus}$ for $t_{\text{disk}} > 100$ Myr. In other tests, they used a steeper slope for $D < 100$ km in an attempt to obtain $\gamma \simeq 2$ as a result of collisional grinding. These tests failed as well for reasons similar to those described above.

Given these unresolved issues, we decided to adopt the following scheme for our nominal simulations of impacts on KBO binaries. We used the reference size distribution ($20 M_{\oplus}$ initially) and switched off the fragmentation of planetesimals ($f_Q \gg 1$). In this case, the size distribution stayed approximately the same over the whole length of the simulation. This is arguably a very conservative assumption. Other schemes would require that the initial population was larger and decayed over time, implying more impacts overall.

Figure 8 shows the survival of equal-size binaries in our nominal simulations. The survival probability is a strong function of the physical size of binary components, their separation, and t_{disk} . Panel (b) is similar to Fig. 2 in Nesvorný et al. (2018), where the results were obtained for the P-M binary ($R_1 + R_2 = 109$ km and $\rho = 0.88$ g cm $^{-3}$; here we use $R_1 + R_2 = 100$ km and $\rho = 1$ g cm $^{-3}$). It shows that the equal size binaries with $R_1 + R_2 = 100$ km are not expected to survive, on average, unless $t_{\text{disk}} < 100$ Myr. Binaries with smaller (larger) components have lower (higher) survival chances, as already noted in Nesvorný et al. (2011) and Parker et al. (2012). The implications of these results for the binary occurrence in the Kuiper belt are discussed in Section 6.

Motivated by the results of Nesvorný et al. (2018), we now consider $t_{\text{disk}} < 100$ Myr (Figures 9 and 10). The rounded shape of the initial size distribution was informed from the hydrodynamical simulations of the streaming instability (Simon et al. 2017). The characteristic size of planetesimals formed by the streaming instability was set to $D = 100$ km. In Fig. 9, we used the initial disk mass $M_{\text{disk}} = 30 M_{\oplus}$ and $f_Q = 0.1$, and let the disk grind for $t_{\text{disk}} = 10$ Myr. In Fig. 10, we adopted $M_{\text{disk}} = 40 M_{\oplus}$, $f_Q = 0.3$ and $t_{\text{disk}} = 50$ Myr. In both these cases, the final size distribution was required to fit the size distribution reconstructed from Jupiter Trojans (Section 4.2) and, indeed, Figures 9 and 10 show that both simulations satisfied this constraint quite well.

The binary survival probability is significantly lower in the case of larger initial disk mass and longer disk lifetime. This is most obvious for binaries with smaller components, $R_1 + R_2 = 30$ km, for which the survival for $M_{\text{disk}} = 40 M_{\oplus}$ and $t_{\text{disk}} = 50$ Myr is roughly 10 times lower than for $M_{\text{disk}} = 30 M_{\oplus}$ and $t_{\text{disk}} = 10$ Myr (compare Figs. 9b and 10b). The lower survival probability is expected because more massive disks with longer lifetimes provide more impactors overall. More massive binaries have better chances of survival. For example, for $R_1 + R_2 = 300$ km and $a_B = 10,000$ km, the survival probability is $\simeq 45\%$ for $M_{\text{disk}} = 40 M_{\oplus}$ and $t_{\text{disk}} = 50$ Myr, and $\simeq 80\%$ for $M_{\text{disk}} = 30 M_{\oplus}$ and $t_{\text{disk}} = 10$ Myr.

The two cases described here (Figs. 10 and 11) are not unique. In fact, there is a continuous range of parameters (initial M_{disk} , t_{disk} , f_Q , etc.) that satisfy the existing constraints (mainly the size distribution inferred from Jupiter Trojans). It is therefore unclear at this point whether the binary survival was higher, such as in Fig. 9, or lower, such as in Fig. 10, or whether some other case not considered here could end up giving a different result. In any case, our results show how the binary occurrence in the hot population of the Kuiper belt is linked to the mass and lifetime of the massive planetesimal disk. Additional work will be needed to resolve this relationship in more detail.

5.4. Collisional Survival During Subsequent Epochs

The massive planetesimal disk below 30 au is dispersed when Neptune migrates into it. A small fraction of disk planetesimals is subsequently implanted into different populations in the Kuiper belt. The exact timing of these events is uncertain, but the P-M binary constraint implies that $t_{\text{disk}} < 100$ Myr (Nesvorný et al. 2018). Examples with $t_{\text{disk}} = 10$ and 50 Myr were discussed in the previous section. Here we adopt $t_{\text{disk}} = 0$ and consider a case when Neptune migrates into the planetesimal disk immediately after t_0 . The impact probability P_i and v_i were evaluated as a function of time as described in Section 4.2 (Figure 11). The changing conditions were implemented in the *Boulder* code, which was then used to determine the collisional survival of binaries over the past 4.5 Gyr.

We found that, to fit the present size distribution of Jupiter Trojans, the shape of the size distribution at $t_0 + t_{\text{disk}}$ must have been similar to the present one for $D > 10$ km (Figure 12a). This is because the impact probability drops relatively fast such that not much grinding

happens for $D > 10$ km over 4.5 Gyr (with $t_{\text{disk}} = 0$). The surviving fraction of equal-size binaries is shown in Figure 12b. The survival probability is sensitive to the size of binary components and their separation. For $R_1 + R_2 = 100\text{-}300$ km, which is the characteristic size of known equal-size binaries, the survival probability is 74-96% for $a_{\text{B}} \simeq 1,000\text{-}10,000$ km. Most of these binaries are therefore expected to survive. A sharp drop-off of the probability at $a_{\text{B}}/(R_1 + R_2) \sim 10^3$ occurs because separations approach $0.5 R_{\text{B,Hill}}$, where $R_{\text{B,Hill}}$ is the binary heliocentric Hill radius (e.g., $R_{\text{B,Hill}} \simeq 250,000$ km for an equal size-binary with $R_1 + R_2 = 100$ km, $\rho = 1$ g cm $^{-3}$ and $a = 30$ au). These very wide binaries are dynamically unstable.

The results shown in Figures 11 and 12 were obtained for the case2 migration parameters (Table 2) and HCs, but the results for case1 and other KBO populations are similar. The survival probability of binaries is sensitive to our assumption about the number of disk planetesimals at $t_0 + t_{\text{disk}}$, which is linked, through the implantation probability, to the number of KBOs. We showed previously (e.g., Nesvorný & Vokrouhlický 2016, Nesvorný et al. 2016) that our baseline dynamical model for the Kuiper belt implantation produces populations that are similar to those inferred from observations of HCs, Plutinos, scattering and detached population. Still, there is some uncertainty in this comparison both on the side of observations (albedo assumptions, survey biases, etc.) and model (dependence on the timescale of Neptune’s migration, number of Pluto-size bodies in the disk, etc.). The initial calibration of the disk population is also uncertain, to within a factor of ~ 2 , because the capture probability of Jupiter Trojans depends on various details of the model setup.

To tentatively account for these uncertainties, we considered cases with $M_{\text{disk}} = 10 M_{\oplus}$ and $30 M_{\oplus}$ (recall that $M_{\text{disk}} = 20 M_{\oplus}$ at $t_0 + t_{\text{disk}}$ in our nominal case). This would correspond to $P_{\text{JT}} = 7.5 \times 10^{-8}$ and 2.5×10^{-8} , respectively (see Section 4.2), which is somewhat outside the range of values favored in Nesvorný et al. (2013), but still potentially plausible. By testing these cases, we found that the survival probabilities of equal size binaries are very similar (within $\sim 20\%$) to those shown in Figure 12b. The results shown in Fig. 12b are therefore relatively robust.

In summary, the overall survival of equal-size binaries mainly depends on the early phase, when the binaries are immersed in the massive planetesimal disk and have to withstand an intense initial bombardment. The magnitude of the initial bombardment depends on M_{disk}

and t_{disk} . The occurrence of binaries in the Kuiper belt could, at least in principle (i.e., after factoring in the effect of planetary encounters; Section 5.1), be therefore used to constrain M_{disk} and t_{disk} (see Section 6 for discussion).

5.5. Kozai Dynamics and Tides

Additional effects that can alter binary orbits, and may therefore influence binary survival, include Kozai dynamics and tides (e.g., Porter & Grundy 2012). The Kozai dynamics of a binary orbit arises due to the gravitational potential of the Sun. For the Kozai cycles to be effective, the binary components must be roughly spherical and/or the binary separation must be large. If not, the gravitational potential from the J_2 term of binary components prevails over the solar gravity, resulting in a simple precession of the binary orbit about the heliocentric orbit pole.

Porter & Grundy (2012) studied these effects, including the tidal dissipation (Goldreich & Sari 2009), and concluded that the combined effect of Kozai cycles and tides can remove binaries with inclinations $i_B \sim 90^\circ$ and $a_B > a_{\text{crit}}$, where a_{crit} depends on J_2 and the strength of tidal dissipation. Given that several known Kuiper belt binaries with $a_B < 0.05 R_{\text{Hill}}$ have $i_B \sim 90^\circ$, this probably implies $a_{\text{crit}} > 0.05 R_{\text{Hill}}$. This reasoning, if applied to the Kuiper belt binaries with $a_B < 0.05 R_{\text{Hill}}$, suggests that these additional effects do not play a major role in their survival. The Kozai cycles and tides probably acted to eliminate binaries with $a_B > 0.05 R_{\text{Hill}}$ and $i_B \sim 90^\circ$ (Grundy et al. 2018).

5.6. Large Primaries with Small Satellites

Our base hypothesis is that the (nearly) *equal*-size binaries with $R_2/R_1 > 0.5$ formed during the earliest stages (Goldreich et al. 2002, Nesvorný et al. 2010). In contrast, it is not quite clear when the *unequal*-size binaries with $R_2/R_1 < 0.5$ formed. They are presumably a by-product of large scale collisions (Canup 2005, Leinhardt et al. 2010). On one hand, the collisional activity is the most intense during the lifetime of the massive disk, before the disk is dispersed by Neptune. On the other hand, there is at least one case where there are good reasons to believe that the satellite-forming collision happened relatively late, that is *after*

the massive disk dispersal. This is the case of two Haumea moons, Hi'iaka and Namaka. Haumea has a collisional family (Brown et al. 2007), which must have formed after the implantation of Haumea onto its current orbit (the family would otherwise be dispersed during implantation). Thus, if Hi'iaka and Namaka formed as a result of the family-forming collision, their formation most likely post-dates the epoch of Neptune's migration.

For unequal-size binaries that formed before the disk dispersal, the dynamical survival probability can be inferred from Figure 3. For example, Charon, Styx and Hydra have $a_B/R_B = 15.8, 34.4$ and 52.3 , respectively.⁶ According to Fig. 3, we find that these moons are expected to survive in 67%, 45% and 31% of cases. In Fig. 3, however, we assumed $\rho = 1 \text{ g cm}^{-3}$, which is not adequate for Pluto ($\rho = 1.9 \text{ g cm}^{-3}$) and Charon ($\rho = 1.7 \text{ g cm}^{-3}$). We therefore opted for simulating the survival of Pluto's moons directly. The results are given in Table 3 (they are roughly consistent with shifting the lines in Fig. 3 by a factor of $(1.8)^{1/3}$ to the right). Charon survives in 91% of trials in the case2 simulation and in 94% of trials in the case1 simulation. This is comforting (see also Pires et al. 2015).

For Hydra, which is the farthest of Pluto's known moons, the survival probabilities are 74% in case2 and 82% in case1. Also, in 41% and 53% of trials, respectively, Hydra ends up with the final orbital eccentricity below 0.01 (this assumes that is started with $e = 0$). For Styx, which is the closest of Pluto's small moons, the eccentricity stays below 0.01 in 56% and 66% of trials. For comparison, the present orbital eccentricities of Hydra and Styx are $\simeq 0.006$ (Showalter & Hamilton 2015). It is plausible that these eccentricities were generated by perturbations during encounters of the Pluto system to Neptune, but the probability of that happening is small (Table 3). In addition, it is possible that Hydra started in the 6:1 resonance with Charon and was displaced from that resonance by planetary encounters. This requires a negative semimajor axis change $\Delta a \simeq -140 \text{ km}$. For comparison, we find that $\Delta a < -100 \text{ km}$ in only $\sim 15\%$ of cases.

Eris and Dysnomia with $a_B/R_B \simeq 31$ show larger survival probabilities than Styx (Eris's density is $\rho = 2.5 \text{ g cm}^{-3}$). Makemake's satellite, known as MK2, has a large orbital uncertainty with semimajor axis ranging between 21,000 and 300,000 km (Parker et al. 2016).

⁶For Styx and Hydra, we define $R_B^3 = R_1^3 + R_2^3$, where R_1 is the effective radius of Pluto and Charon ($\simeq 1238 \text{ km}$).

This would give $a_B/R_B \simeq 29\text{-}410$. The cases with $a_B/R_B > 100$ can probably be ruled out because the survival odds are $\lesssim 10\%$ for these large separations. Quaoar-Weywot and Orcus-Vanth have $a_B/R_B \simeq 26$ and 19 , respectively, and are safe ($>50\%$ survival probabilities according to Figure 3, but this is a generous lower limit given that, for example, Orcus density is $\rho = 1.5 \text{ g cm}^{-3}$). In summary, we find that all known satellites of the largest KBOs are likely to survive during the dynamical implantation of these bodies in the Kuiper belt.

We performed several tests to understand the effect of impacts on unequal size binaries. For example, we considered the small satellites of Pluto during and after the phase of the massive disk dispersal (i.e., the case with $t_{\text{disk}} = 0$). These tests closely followed the setup described in Section 5.4 (see Fig. 12a). All moons were started on circular orbits. We found that the survival probability of all small Pluto moons is very nearly 100%. As for Hydra, the characteristic change of the semimajor axis and eccentricity due to impacts is only $\sim 100 \text{ km}$ and 0.001 , too low to explain Hydra’s current orbital eccentricity ($\simeq 0.006$). The results for Kerberos are similar, but Kerberos’s eccentricity is smaller ($\simeq 0.003$). For example, in about 30% of cases, Kerberos ends up with $e > 0.0015$ (i.e. at least a half of its present eccentricity). Larger effects are expected for $t_{\text{disk}} > 0$. This shows that at least some of Pluto’s moons (not Charon) may owe their slightly excited orbits to small impacts.

6. Discussion

6.1. Contact and Very Tight Binaries

The equal-size ($R_2/R_1 > 0.5$) binaries in the hot population can be divided into several categories. The contact and very tight binaries with $a_B/R_B < 10$, such as 2001 QG298 and the inner pair of (47171) Lempo, are difficult to detect observationally. Here we showed that $\simeq 10\%$ of equal-size binaries are expected to collapse into contact binaries during the implantation of objects into the Kuiper belt (Fig. 3). In addition, $\sim 10\text{-}30\%$ of equal-size binaries are expected to collapse into contact binaries during the collisional evolution of the massive disk (Nesvorný et al. 2018). Assuming a 100% initial binary fraction, these results imply that the fraction of contact binaries in the hot population should be of the order of 10-30%. For comparison, Sheppard & Jewitt (2004) proposed from the detection

of 2001 QG298 (contact binary in the Plutino population) that at least $\sim 10\%$ of KBOs are contact binaries, and Thirouin & Sheppard (2018) suggested that up to $\sim 40\%$ Plutinos can be contact binaries. The contact binary fraction among CCs remains to be determined, but if the main channel of contact binary formation is binary collapse from impact and planetary encounter perturbations, the contact binary fraction among ~ 100 -km-class CCs is expected to be low (most large CC binaries presumably survived). Recent observations of (486958) 2014 MU69 by the New Horizons spacecraft show that contact binaries may be common among smaller, ~ 10 -km-class CCs.

6.2. Tight Binaries

The tightly-bound binaries with $10 < a_B/R_B < 30$ have $> 50\%$ dynamical survival probability (Fig. 3) and do not provide a useful constraint on the implantation process itself. The nine known binaries with $10 < a_B/R_B < 30$ represent a fraction of $\sim 3\%$ of dynamically hot KBOs that were searched for binaries with the Hubble Space Telescope (HST; W. Grundy, personal communication; roughly 300 hot KBOs were imaged by the HST). Some tight binaries may remain unresolved. Thus, as a lower limit, we can estimate that at least $\sim 6\%$ of the massive disk planetesimals were equal-size binaries with $10 < a_B/R_B < 30$. This is similar to the fraction of $a_B/R_B < 10$ binaries inferred from the P-M binary constraint (Nesvorný et al. 2018). Moreover, since the initial fraction of $10 < a_B/R_B < 30$ binaries cannot exceed 100%, their survival probability during the collisional grinding of the massive planetesimal disk cannot be much lower than ~ 0.06 . This constraint implies $t_{\text{disk}} < 100$ Myr (Fig. 8). It means that the massive planetesimal disk must have been dispersed by migrating planets within $\lesssim 100$ Myr after t_0 (Nesvorný et al. 2018).

6.3. Wide Binaries

The wide binaries with $30 < a_B/R_B < 100$ have ~ 10 -50% dynamical survival probability (Fig. 3). There are five known binaries in this category in the hot population (2001 KP76, 2004 PB108, 2006 SF369, 2001 FM185 and the outer component of (47171) Lempo; Table 1), representing a fraction of $\sim 2\%$ of all HST targets in the hot population. This implies the

original fraction of at least $\sim 6\%$, which is similar to the minimal binary fractions found for $a_B/R_B < 10$ and $10 < a_B/R_B < 30$. Together, we infer that at least $\sim 18\%$ of the massive disk planetesimals were equal-size binaries with $a_B/R_B < 100$. Lower fractions would be inferred from the present analysis if 2001 KP76, 2001 FM185, and possibly (47171) Lempo, turn out to be interlopers from the CC population (these objects have small heliocentric inclinations and may have evolved to their current orbits from $a > 30$ au).

6.4. Very Wide Binaries

Finally, there are four known equal-size binaries in the hot population with $a_B/R_B > 100$ (1998 WW31, 2002 VF130 and 2004 KH19, all HCs, and Mors-Somnus in the Plutino population). These very wide binaries are puzzling because, according to Fig. 3, they have a very low chance of survival during their implantation into the Kuiper belt. 1998 WW31, however, has a heliocentric orbit with low inclination ($i \simeq 7^\circ$) and we are therefore not confident whether it really formed in the massive disk below 30 au; it may be an interloper from the cold population. Similarly, (341520) Mors-Somnus with $i \simeq 11^\circ$ may have been swept into the 3:2 resonance from its original formation location at ~ 35 -39 au (Nesvorný 2015). If so, this binary could have avoided perturbations during planetary encounters.

2004 KH19 and 2002 VF130, whose classification as hot KBOs is secure, only have 8% and 0.8% dynamical survival probabilities (Fig. 3). This could potentially imply a large fraction of the very wide binaries in the original disk. For example, from 2002 VF130, we could infer that the fraction of equal-size binaries with $a_B/R_B \sim 300$ in the original disk was $\sim 40\%$. And that's without factoring in the survival probability during the collisional grinding of the massive disk (Fig. 8b) in which 2002 VF130 presumably formed.

6.5. Comparison of Cold and Hot Binaries

Figure 13 offers a different perspective on the same issue. There we compare the separations of equal-size binaries in the cold and hot populations. The hot population shows a tail of contact and very tight binaries with $a_B/R_B < 10$. These binaries are difficult to detect in the cold population, because of their greater heliocentric distance. If the binaries

with $a_B/R_B < 10$ are removed from the hot population, the separations of hot and cold binaries appear to follow the same trend, except that the cold population has nearly 20% of equal-size binaries with $a_B/R_B > 350$. These extremely wide binaries are missing in the hot population either because they did not form or because they were disrupted by impacts and planetary encounters.

Now, the binaries with $100 < a_B/R_B < 350$ found in the hot population represent a problem, because they should have been removed by planetary encounters as well. To demonstrate this we use the equal-size binaries in the cold population as a template and factor in the dynamical survival probability from Fig. 3. The result is plotted as the “model” distribution in Fig. 13. Indeed, this simple test shows that the binaries with $100 < a_B/R_B < 350$ should have been nearly completely removed from the hot population, while in reality they represent $\sim 16\%$ of cases (4 out of 25).

This may mean one of several things. It may indicate, for example, that at least some fraction of hot KBOs reached their current orbits without experiencing planetary encounters. For that to work, these KBOs would have to start beyond the reach of Neptune at >30 au, where they would only be affected by resonances with Neptune (Hahn & Malhotra 2005), which are known to preserve binarity (Fraser et al. 2017). This scenario appears plausible for 1998 WW31 and (341520) Mors-Somnus, which have relatively low heliocentric orbit inclinations. It remains to be shown, however, whether this could explain 2002 VF130 ($i = 19.5^\circ$) as well. Unfortunately, the binary semimajor axis of 2002 VF130, estimated from the discovery image (Noll et al. 2009), remains uncertain and no additional astrometry is currently available.

7. Conclusions

We determined the dynamical and collisional survival of KBO binaries before and after their implantation into the dynamically hot population in the Kuiper belt. The main results are:

1. The binary survival is a strong function of the size and separation of binary components. The dynamical survival during scattering encounters with planets only depends on

a_B/R_B , where a_B is the binary semimajor axis and $R_B^3 = R_1^3 + R_2^3$, with R_1 and R_2 being the radii of binary components. The tight binaries with $a_B/R_B < 30$ are expected to survive in $>50\%$ of cases, whereas the wide binaries with $a_B/R_B > 100$ are expected to die in $>90\%$ of cases (Fig. 3).

2. The existence of equal-size binaries in the dynamically hot population of the Kuiper belt implies that the massive planetesimal disk below 30 au was short-lived ($t_{\text{disk}} < 100$ Myr; see also Nesvorný et al. 2018). The disk could have started with a rounded size distribution of planetesimals, as indicated by the streaming instability simulations (e.g., Simon et al. 2017), and $M_{\text{disk}} > 20 M_{\oplus}$. It would subsequently collisionally evolve, within $\sim 10\text{-}50$ Myr, to a size distribution similar to that of Jupiter Trojans and $M_{\text{disk}} \simeq 15\text{-}20 M_{\oplus}$ (Figs. 9 and 10). The size distribution and binary fraction are not expected to change much after the implantation of objects into the Kuiper belt (Fig. 12).
3. The initial fraction of tight equal-size binaries in the massive disk should have been at least $\sim 18\%$ for $a_B/R_B < 100$ to account for the present population of equal-size binaries among the hot KBOs. The extremely wide equal-size binaries with $a_B/R_B > 350$ have been removed during the implantation process (< 0.003 survival probability). The existence of wide equal-size binaries with $100 < a_B/R_B < 350$ in the hot population is puzzling. They may be survivors of a much larger original population of wide binaries in the massive disk, or, at least in some cases, are interlopers from the dynamically cold population. 2002 VF130 with the heliocentric orbit inclination $i = 19.5^\circ$ and estimated $a_B/R_B \sim 310$ is an important constraint on the implantation process.
4. All known satellites of the largest KBOs are expected to survive during the dynamical implantation of their primaries in the Kuiper belt. Most of them likely formed during the early stages when their parent bodies were immersed in the massive planetesimal disk below 30 au and sustained intense bombardment. The low orbital eccentricities of Pluto’s small moons may have been excited during encounters of the Pluto system to Neptune, or by small impacts during the massive disk lifetime.
5. The expected fraction of contact binaries from the population of collapsed equal-size binaries is $\sim 10\text{-}30\%$ (this estimate assumes that all planetesimals formed as binaries),

whereas the observational constraints indicate that the contact binary fraction among hot KBOs is $\sim 10\text{-}40\%$ (Sheppard & Jewitt 2004, Thirouin & Sheppard 2018).

We thank W. Grundy and K. Noll for the list of KBOs that were imaged by the HST. The work of D.N. was supported by the NASA Emerging Worlds program. The work of D.V. was supported by the Czech Science Foundation (grant 18-06083S). We thank J.-M. Petit and an anonymous reviewer for helpful corrections of the submitted manuscript.

REFERENCES

- Agnor, C. B., Hamilton, D. P. 2006. Neptune’s capture of its moon Triton in a binary-planet gravitational encounter. *Nature* 441, 192-194.
- Batygin, K., Brown, M. E., Fraser, W. C. 2011. Retention of a Primordial Cold Classical Kuiper Belt in an Instability-Driven Model of Solar System Formation. *The Astrophysical Journal* 738, 13.
- Benz, W., Asphaug, E. 1999. Catastrophic Disruptions Revisited. *Icarus* 142, 5-20.
- Bernstein, G. M., Trilling, D. E., Allen, R. L., Brown, M. E., Holman, M., Malhotra, R. 2004. The Size Distribution of Trans-Neptunian Bodies. *The Astronomical Journal* 128, 1364-1390.
- Bottke, W. F., Walker, R. J., Day, J. M. D., Nesvorný, D., Elkins-Tanton, L. 2010. Stochastic Late Accretion to Earth, the Moon, and Mars. *Science* 330, 1527.
- Brown, M. E. 2001. The Inclination Distribution of the Kuiper Belt. *Astronomical Journal* 121, 2804-2814.
- Brown, M. E., Barkume, K. M., Ragozzine, D., Schaller, E. L. 2007. A collisional family of icy objects in the Kuiper belt. *Nature* 446, 294-296.
- Brucker, M. J., Grundy, W. M., Stansberry, J. A., Spencer, J. R., Sheppard, S. S., Chiang, E. I., Buie, M. W. 2009. High albedos of low inclination Classical Kuiper belt objects. *Icarus* 201, 284-294.

- Canup, R. M. 2005. A Giant Impact Origin of Pluto-Charon. *Science* 307, 546-550.
- Durda, D. D., Bottke, W. F., Nesvorný, D., Enke, B. L., Merline, W. J., Asphaug, E., Richardson, D. C. 2007. Size-frequency distributions of fragments from SPH/ N-body simulations of asteroid impacts: Comparison with observed asteroid families. *Icarus* 186, 498-516.
- Fraser, W. C., Brown, M. E., Morbidelli, A., Parker, A., Batygin, K. 2014. The Absolute Magnitude Distribution of Kuiper Belt Objects. *The Astrophysical Journal* 782, 100.
- Fraser, W. C., and 21 colleagues 2017. All planetesimals born near the Kuiper belt formed as binaries. *Nature Astronomy* 1, 0088.
- Gladman, B., Marsden, B. G., Vanlaerhoven, C. 2008. Nomenclature in the Outer Solar System. *The Solar System Beyond Neptune* 43-57.
- Goldreich, P., Sari, R. 2009. Tidal Evolution of Rubble Piles. *The Astrophysical Journal* 691, 54-60.
- Goldreich, P., Lithwick, Y., Sari, R. 2002. Formation of Kuiper-belt binaries by dynamical friction and three-body encounters. *Nature* 420, 643-646.
- Gomes, R. S., Morbidelli, A., Levison, H. F. 2004. Planetary migration in a planetesimal disk: why did Neptune stop at 30 AU? *Icarus* 170, 492-507.
- Greenberg, R. 1982. Orbital interactions - A new geometrical formalism. *The Astronomical Journal* 87, 184-195.
- Grundy, W. M. et al. (2018). Mutual orbits of binaries in the Kuiper belt. *Transneptunian Solar System Conference*, 26-28 March, 2018, Coimbra, Portugal.
- Gulbis, A. A. S., Elliot, J. L., Adams, E. R., Benecchi, S. D., Buie, M. W., Trilling, D. E., Wasserman, L. H. 2010. Unbiased Inclination Distributions for Objects in the Kuiper Belt. *The Astronomical Journal* 140, 350-369.
- Hahn, J. M., Malhotra, R. 2005. Neptune's Migration into a Stirred-Up Kuiper Belt: A Detailed Comparison of Simulations to Observations. *The Astronomical Journal* 130, 2392-2414.

- Johnston, W. R. 2018. Binary Minor Planets Compilation V2.0. NASA Planetary Data System 305.
- Kaib, N. A., Sheppard, S. S. 2016. Tracking Neptune’s Migration History through High-perihelion Resonant Trans-Neptunian Objects. *The Astronomical Journal* 152, 133.
- Kenyon, S. J., Bromley, B. C. 2001. Gravitational Stirring in Planetary Debris Disks. *The Astronomical Journal* 121, 538-551.
- Lawler, S. M., and 10 colleagues 2018. OSSOS: XIII. Fossilized Resonant Dropouts Imply Neptune’s Migration was Grainy and Slow. arXiv e-prints arXiv:1808.02618.
- Leinhardt, Z. M., Stewart, S. T. 2009. Full numerical simulations of catastrophic small body collisions. *Icarus* 199, 542-559.
- Leinhardt, Z. M., Marcus, R. A., Stewart, S. T. 2010. The Formation of the Collisional Family Around the Dwarf Planet Haumea. *The Astrophysical Journal* 714, 1789-1799.
- Levison, H. F., Duncan, M. J. 1994. The long-term dynamical behavior of short-period comets. *Icarus* 108, 18-36.
- Levison, H. F., Morbidelli, A., Vanlaerhoven, C., Gomes, R., Tsiganis, K. 2008 (L08). Origin of the structure of the Kuiper belt during a dynamical instability in the orbits of Uranus and Neptune. *Icarus* 196, 258-273.
- Levison, H. F., Bottke, W. F., Gounelle, M., Morbidelli, A., Nesvorný, D., Tsiganis, K. 2009. Contamination of the asteroid belt by primordial trans-Neptunian objects. *Nature* 460, 364-366.
- Levison, H. F., Morbidelli, A., Tsiganis, K., Nesvorný, D., Gomes, R. 2011. Late Orbital Instabilities in the Outer Planets Induced by Interaction with a Self-gravitating Planetary Disk. *The Astronomical Journal* 142, 152.
- Morbidelli, A., Rickman, H. 2015. Comets as collisional fragments of a primordial planetesimal disk. *Astronomy and Astrophysics* 583, A43.
- Morbidelli, A., Levison, H. F., Tsiganis, K., Gomes, R. 2005. Chaotic capture of Jupiter’s Trojan asteroids in the early Solar System. *Nature* 435, 462-465.

- Morbidelli, A., Levison, H. F., Bottke, W. F., Dones, L., Nesvorný, D. 2009. Considerations on the magnitude distributions of the Kuiper belt and of the Jupiter Trojans. *Icarus* 202, 310-315.
- Nesvorný, D. 2015. Jumping Neptune Can Explain the Kuiper Belt Kernel. *The Astronomical Journal* 150, 68.
- Nesvorný, D., Morbidelli, A. 2012 (NM12). Statistical Study of the Early Solar System's Instability with Four, Five, and Six Giant Planets. *The Astronomical Journal* 144, 117.
- Nesvorný, D., Vokrouhlický, D. 2016. Neptune's Orbital Migration Was Grainy, Not Smooth. *The Astrophysical Journal* 825, 94.
- Nesvorný, D., Youdin, A. N., Richardson, D. C. 2010 (NYR10). Formation of Kuiper Belt Binaries by Gravitational Collapse. *The Astronomical Journal* 140, 785-793.
- Nesvorný, D., Vokrouhlický, D., Bottke, W. F., Noll, K., Levison, H. F. 2011. Observed Binary Fraction Sets Limits on the Extent of Collisional Grinding in the Kuiper Belt. *The Astronomical Journal* 141, 159.
- Nesvorný, D., Vokrouhlický, D., Morbidelli, A. 2013. Capture of Trojans by Jumping Jupiter. *The Astrophysical Journal* 768, 45.
- Nesvorný, D., Vokrouhlický, D., Roig, F. 2016. The Orbital Distribution of Trans-Neptunian Objects Beyond 50 au. *The Astrophysical Journal* 827, L35.
- Nesvorný, D., Vokrouhlický, D., Bottke, W. F., Levison, H. F. 2018. Evidence for very early migration of the Solar System planets from the Patroclus-Menoetius binary Jupiter Trojan. *Nature Astronomy* .
- Noll, K. S., Levison, H. F., Grundy, W. M., Stephens, D. C. 2006. Discovery of a binary Centaur. *Icarus* 184, 611-618.
- Noll, K. S., Grundy, W. M., Chiang, E. I., Margot, J.-L., Kern, S. D. 2008a. Binaries in the Kuiper Belt. *The Solar System Beyond Neptune* 345-363.

- Noll, K. S., Grundy, W. M., Stephens, D. C., Levison, H. F., Kern, S. D. 2008b. Evidence for two populations of classical transneptunian objects: The strong inclination dependence of classical binaries. *Icarus* 194, 758-768.
- Noll, K. S., Benecchi, S. D., Grundy, W. M. 2009. 2002 VF130. *International Astronomical Union Circular* 9040, 1.
- Parker, A. H., Kavelaars, J. J. 2010. Destruction of Binary Minor Planets During Neptune Scattering. *The Astrophysical Journal* 722, L204-L208.
- Parker, A. H., Kavelaars, J. J. 2012. Collisional Evolution of Ultra-wide Trans-Neptunian Binaries. *The Astrophysical Journal* 744, 139.
- Parker, A. H., Buie, M. W., Grundy, W. M., Noll, K. S. 2016. Discovery of a Makemakean Moon. *The Astrophysical Journal* 825, L9.
- Petit, J.-M., Mousis, O. 2004. KBO binaries: how numerous were they? *Icarus* 168, 409-419.
- Pires, P., Giuliatti Winter, S. M., Gomes, R. S. 2015. The evolution of a Pluto-like system during the migration of the ice giants. *Icarus* 246, 330-338.
- Porter, S. B., Grundy, W. M. 2012. KCTF evolution of trans-neptunian binaries: Connecting formation to observation. *Icarus* 220, 947-957.
- Press, W. H., Teukolsky, S. A., Vetterling, W. T., Flannery, B. P. 1992. *Numerical recipes in FORTRAN. The art of scientific computing*. Cambridge: University Press, 1992, 2nd ed.
- Shannon, A., Dawson, R. 2018. Limits on the number of primordial Scattered disc objects at Pluto mass and higher from the absence of their dynamical signatures on the present-day trans-Neptunian Populations. *Monthly Notices of the Royal Astronomical Society* 480, 1870-1882.
- Sheppard, S. S., Jewitt, D. 2004. Extreme Kuiper Belt Object 2001 QG₂₉₈ and the Fraction of Contact Binaries. *The Astronomical Journal* 127, 3023-3033.
- Showalter, M. R., Hamilton, D. P. 2015. Resonant interactions and chaotic rotation of Pluto's small moons. *Nature* 522, 45-49.

- Simon, J. B., Armitage, P. J., Youdin, A. N., Li, R. 2017. Evidence for Universality in the Initial Planetesimal Mass Function. *The Astrophysical Journal* 847, L12.
- Singer, K. N., McKinnon, W. B., Gladman, B., et al., 2019. Impact Craters on Pluto and Charon Reveal a Deficit of Small Kuiper Belt Objects. *Science*, in press.
- Tegler, S. C., Romanishin, W. 2000. Extremely red Kuiper-belt objects in near-circular orbits beyond 40 AU. *Nature* 407, 979-981.
- Thirouin, A., Sheppard, S. S. 2018. The Plutino Population: An Abundance of Contact Binaries. *The Astronomical Journal* 155, 248.
- Veillet, C., Parker, J. W., Griffin, I., Marsden, B., Doressoundiram, A., Buie, M., Tholen, D. J., Connelley, M., Holman, M. J. 2002. The binary Kuiper-belt object 1998 WW31. *Nature* 416, 711-713.
- Vilenius, E., and 16 colleagues 2014. “TNOs are Cool”: A survey of the trans-Neptunian region. X. Analysis of classical Kuiper belt objects from Herschel and Spitzer observations. *Astronomy and Astrophysics* 564, A35.
- Weidenschilling, S. J., Spaute, D., Davis, D. R., Marzari, F., Ohtsuki, K. 1997. Accretional Evolution of a Planetesimal Swarm. *Icarus* 128, 429-455.
- Wetherill, G. W. 1967. Collisions in the Asteroid Belt. *Journal of Geophysical Research* 72, 2429.
- Wong, I., Brown, M. E. 2015. The Color-Magnitude Distribution of Small Jupiter Trojans. *The Astronomical Journal* 150, 174.
- Yoshida, F., Terai, T. 2017. Small Jupiter Trojans Survey with the Subaru/Hyper Suprime-Cam. *The Astronomical Journal* 154, 71.

number	temp. id.	name	KBO class	$R_1 + R_2$ (km)	a_B (km)	a_B/R_B
(341520)	2007 TY430	Mors-Somnus	Plu	100	21,000	335
–	2002 VF130	–	HC	113	22,400	310
–	1998 WW31	–	HC	135	22,620	263
–	2004 KH19	–	HC	154	13,000	130
(119067)	2001 KP76	–	HC	150	8,900	94
–	2004 PB108	–	HC	187	10,400	81
(47171)	1999 TC36	Lempo	Plu	202	7,411	50
(82157)	2001 FM185	–	Plu	129	3,130	38
–	2006 SF369	–	SDO	142	3,120	35

Table 1: The wide, equal-size binaries in the hot population of the Kuiper belt (HC stands for Hot Classical, Plu for Plutino, SDO for a scattered disk object). For (47171) Lempo (1999 TC36), which is a triple system, we list parameters of the outer component. All these binaries, except for 1998 WW31 (Veillet et al. 2002), were imaged by the Hubble Space Telescope (Noll et al. 2008a,b; Grundy et al. 2018).

	τ_1	τ_2	N_{Pluto}
	(Myr)	(Myr)	
case1	30	100	4000
case2	10	30	2000

Table 2: A two stage migration of Neptune was adopted from Nesvorný & Vokrouhlický (2016): τ_1 and τ_2 define the e -folding exponential migration timescales during these stages, and N_{Pluto} is the assumed number of Pluto-mass objects in the massive disk below 30 au. Neptune’s migration is grainy with these objects as needed to explain the observed proportion of resonant and non-resonant populations in the Kuiper belt.

	Charon	Styx	Hydra
–case1–			
survive	0.94	0.87	0.82
$e < 0.1$	0.88	0.74	0.66
$e < 0.01$	0.82	0.66	0.53
$0.003 < e < 0.012$	–	0.04	0.04
–case2–			
survive	0.91	0.82	0.74
$e < 0.1$	0.83	0.67	0.56
$e < 0.01$	0.75	0.56	0.41
$0.003 < e < 0.012$	–	0.05	0.05

Table 3: The survival probability and orbital changes of Pluto’s moons against dynamical perturbations during planetary encounters. The rows show the probability to satisfy different criteria. The results for Nix and Kerberos are intermediate between those of Styx and Hydra. See Table 2 for definition of cases 1 and 2.

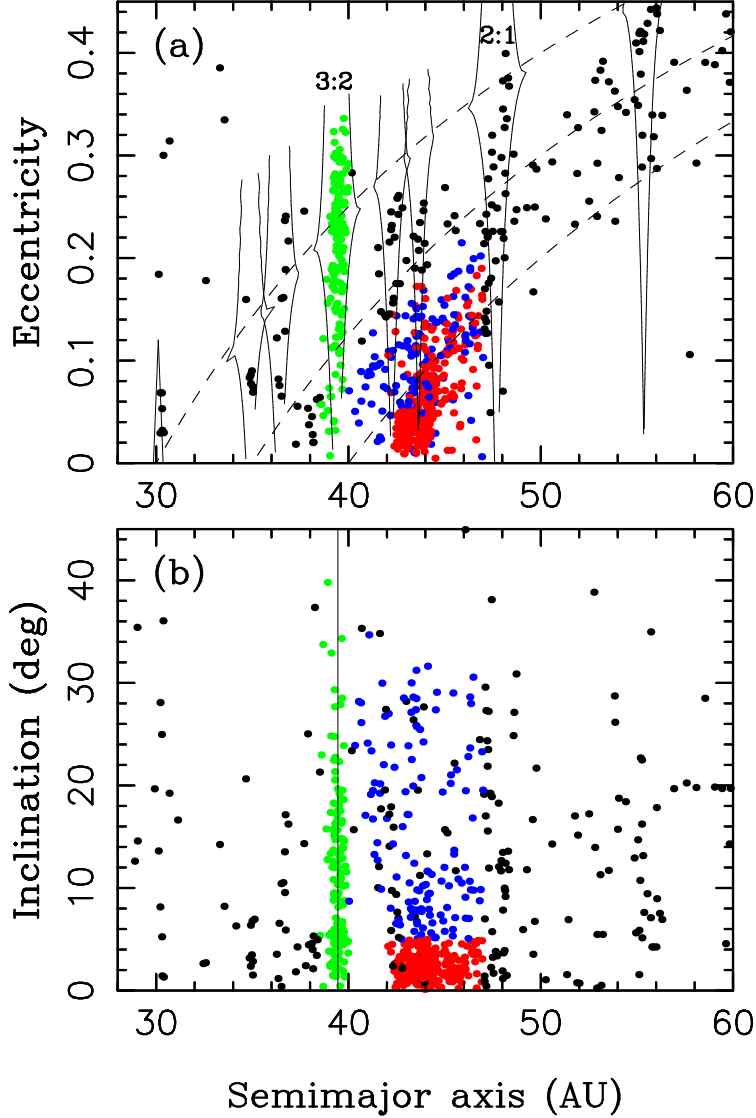


Fig. 1.— The orbits of KBOs observed in three or more oppositions. Various dynamical classes are highlighted. HCs with $i > 5^\circ$ are denoted by blue dots, and CCs with $i < 5^\circ$ are denoted by red dots. The solid lines in panel (a) follow the borders of important orbital resonances. Plutinos in the 3:2 resonance are highlighted by green dots. The dashed lines in panel (a) correspond to $q = a(1 - e) = 30, 35$ and 40 au . See section 4.1 for definitions of different dynamical classes.

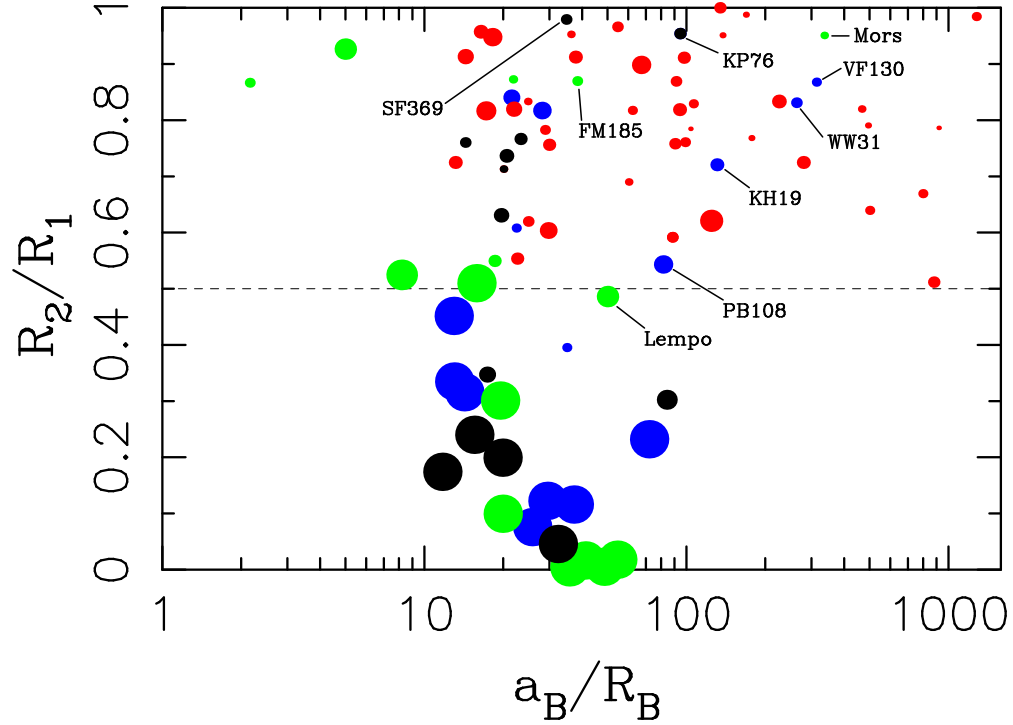


Fig. 2.— The properties of KBO binaries. The color code indicates the relationship of binaries to different dynamical classes (red for CCs, green for Plutinos, blue for HCs, black for everything else; see Fig. 1). The symbol size correlates with the primary diameter. The unequal-size binaries with a large primary and a small moon ($R_2/R_1 < 0.5$) are detected around large primaries in the dynamically hot populations. Most known equal-size binaries ($R_2/R_1 > 0.5$) are in the cold population.

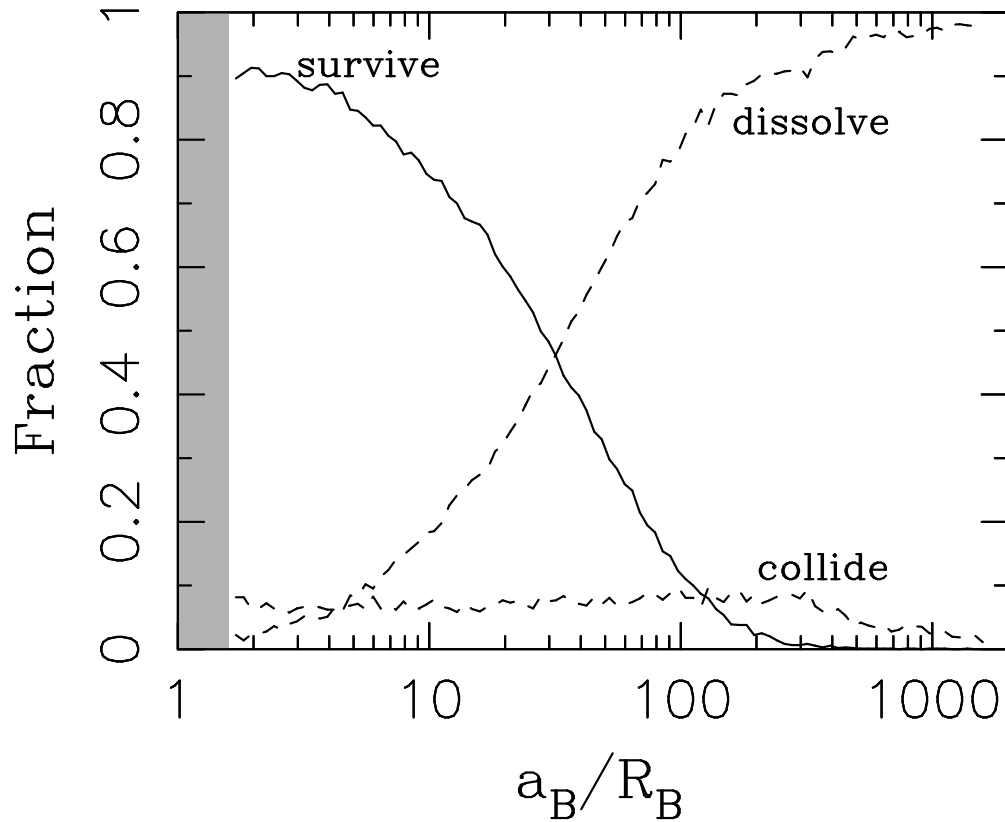


Fig. 3.— The dynamical survival of equal-size binaries that end up in the HC population (solid line). For example, 50% of binaries survive for $a_B/R_B \simeq 28$ and 10% survive for $a_B/R_B \simeq 110$. The dashed lines show the fractions of binaries whose components become unbound or end up colliding with each other. The gray area denotes separations for which the binary components are in contact ($a_B/R_B < 2^{2/3}$).

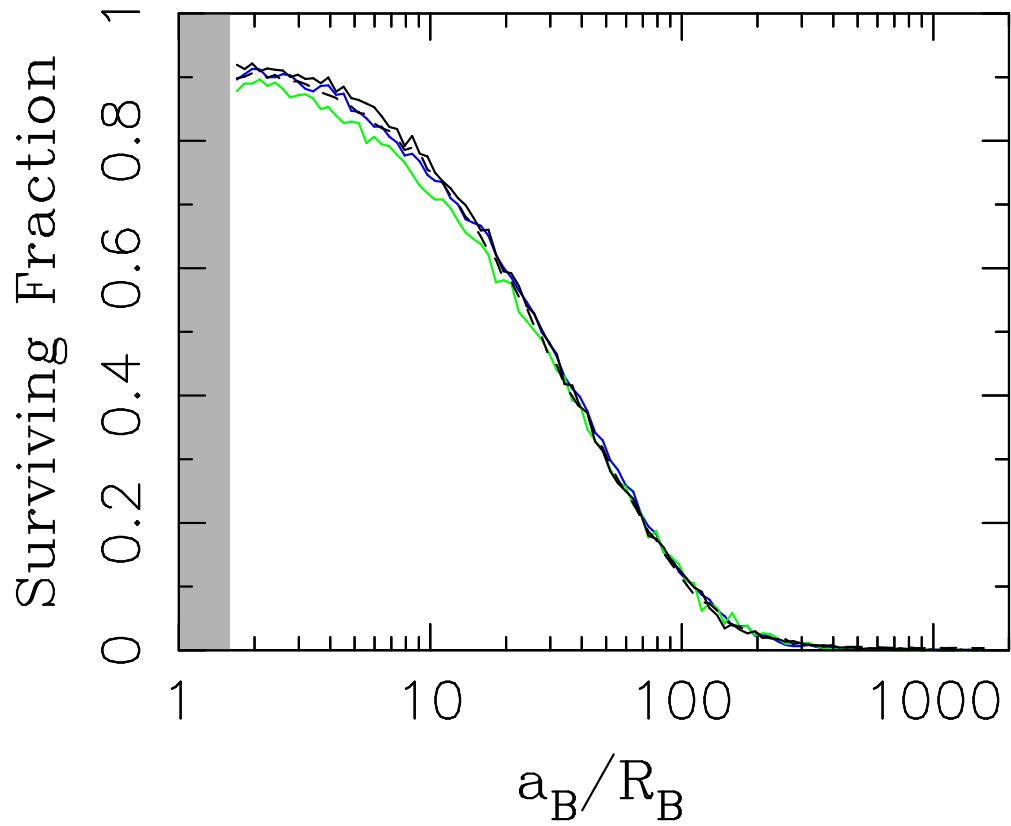


Fig. 4.— The dynamical survival of equal-size binaries in different KBO populations: HCs (blue), Plutinos (green), scattering (solid black) and detached (dashed black) objects. The results obtained for different populations are very similar. The gray area denotes separations for which the binary components are in contact.

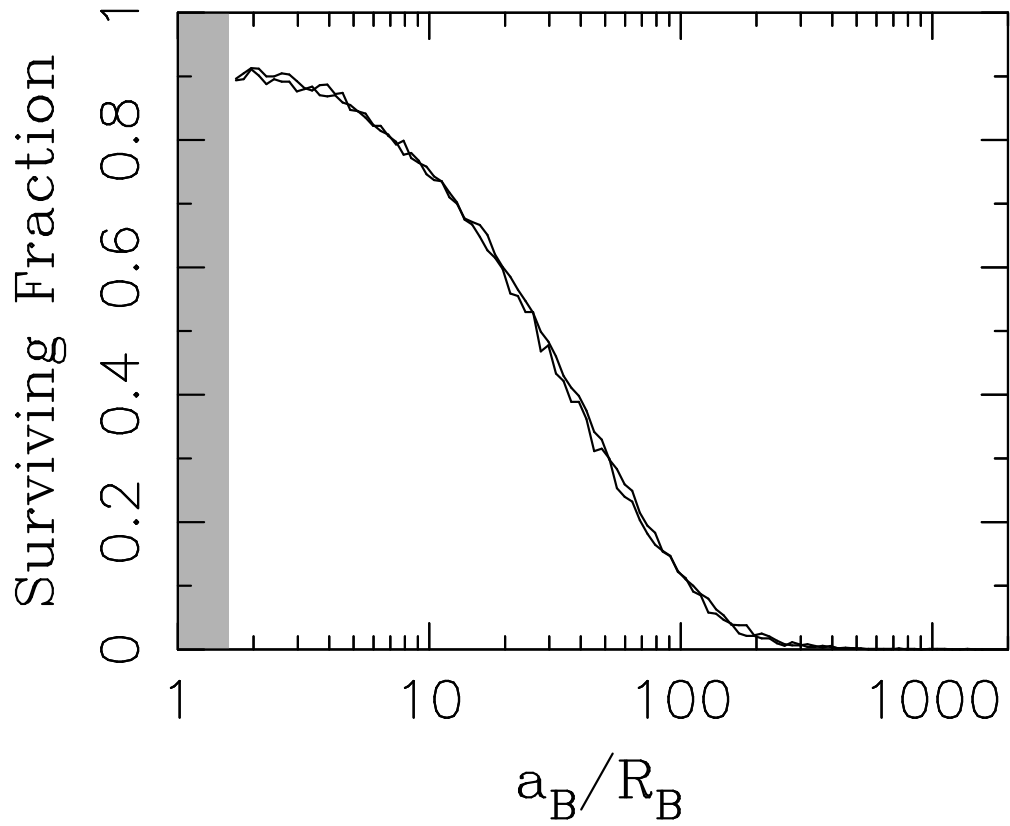


Fig. 5.— The dynamical survival of equal-size binaries implanted into the HC population. The solid curves show results for two different migration histories of Neptune (Table 1). The results are very similar. The gray area denotes separations for which the binary components are in contact.

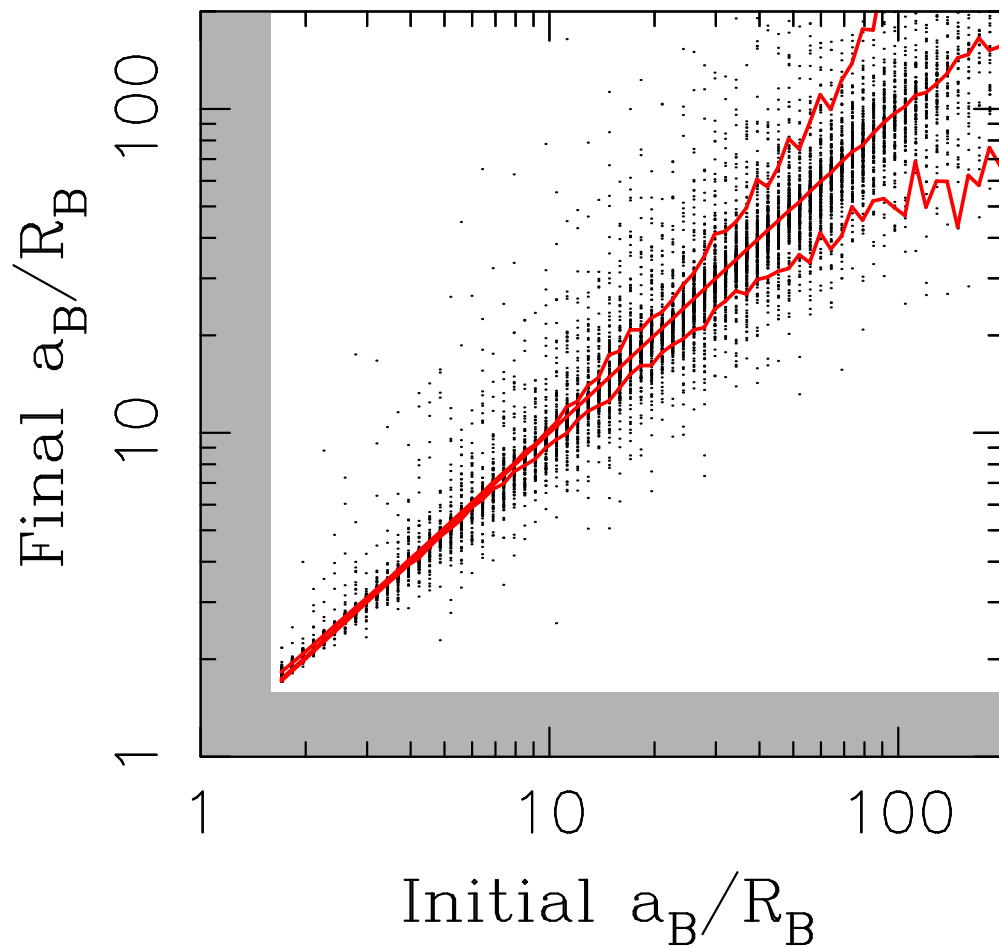


Fig. 6.— The relationship between the initial and final separations of binary orbits in our simulations of planetary encounters. Only binaries surviving the whole sequence of encounters are shown here. The black dots show individual cases. The red lines show the mean, and 5 and 95 percentiles. The gray area denotes separations for which the binary components are in contact. These results were obtained for the case2 migration parameters and HCs.

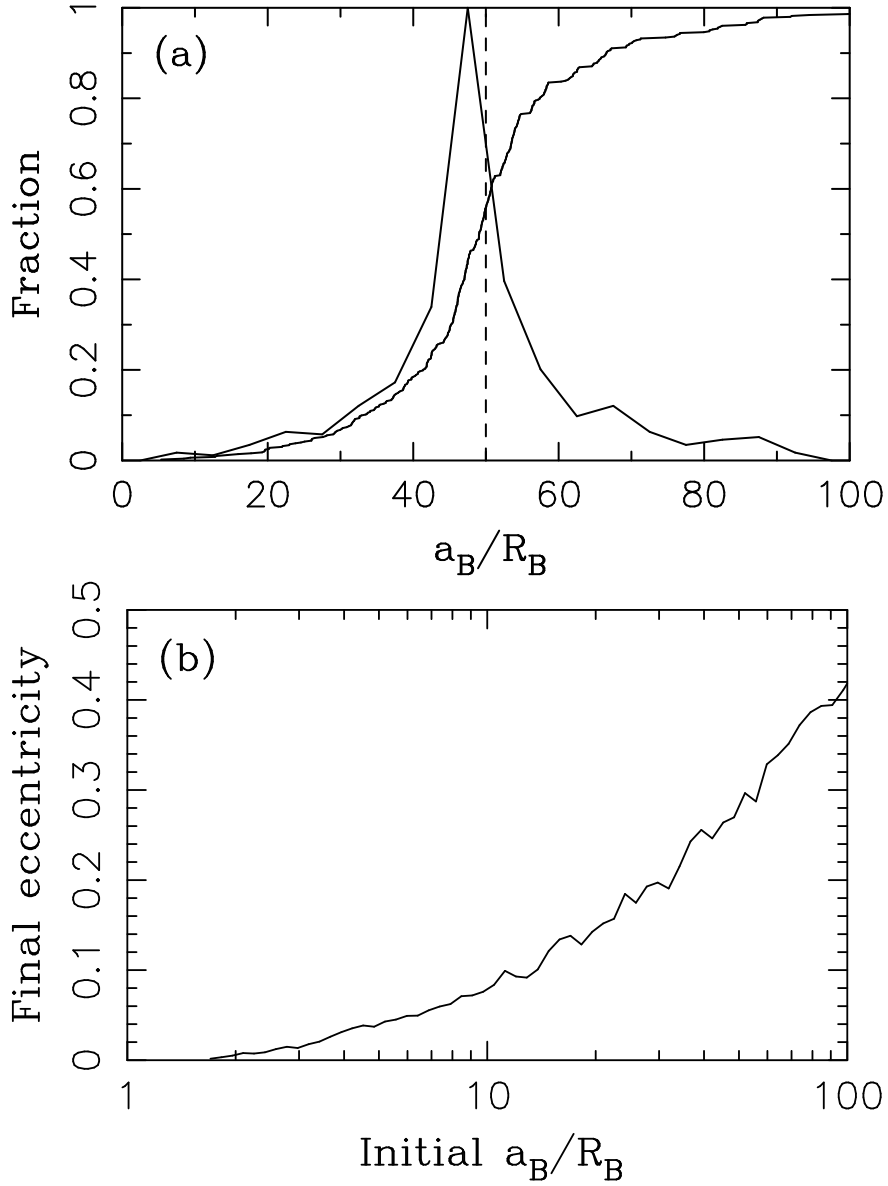


Fig. 7.— The effect of planetary encounters on binary orbits. In panel (a), all binaries started with $a_B/R_B = 50$ (dashed line). The solid lines show the differential and cumulative distributions of a_B/R_B of the final orbits. In panel (b), the final mean eccentricity of binary orbits ($e_B = 0$ initially) is shown as a function of initial a_B/R_B . The plotted eccentricity value was computed by averaging over all surviving binary orbits that started with the corresponding separation. The results were obtained for the case2 migration parameters and HCs.

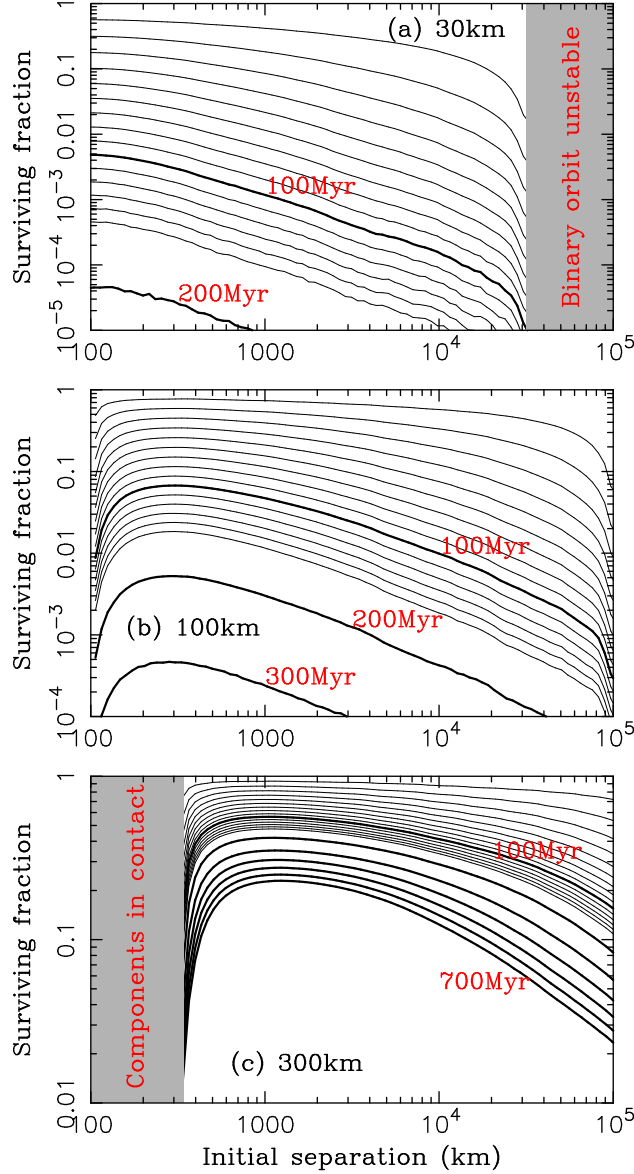


Fig. 8.— The collisional survival of equal-size binaries in our nominal simulations of the massive planetesimal disk. The panels illustrate the results for $R_1 + R_2 = 30$ km (a), 100 km (b) and 300 km (c). The lines show the surviving fraction of binaries for different assumptions on the planetesimal disk lifetime, t_{disk} (thin lines are spaced by 10 Myr up to $t_{\text{disk}} = 150$ Myr, bold lines each 100 Myr).

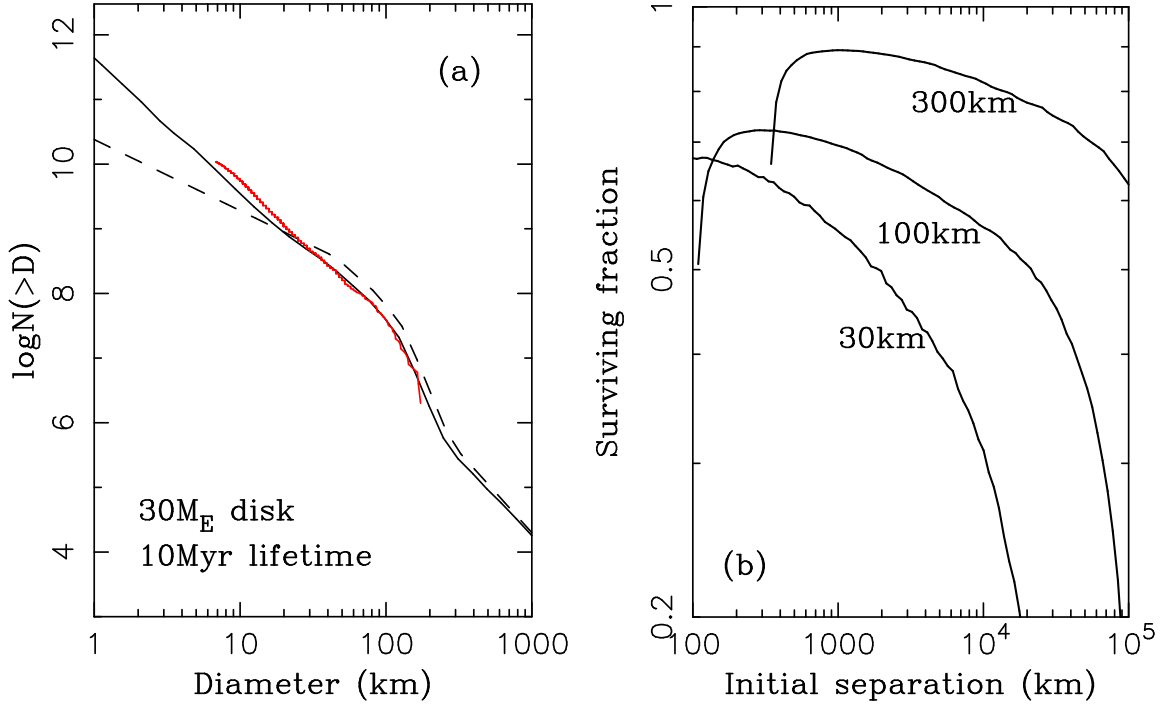


Fig. 9.— Panel (a): collisional evolution of the outer planetesimal disk. The dashed line shows the initial size distribution. It corresponds to the initial disk mass $M_{\text{disk}} = 30 M_{\oplus}$. The solid line shows the size distribution after 10 Myr of collisional grinding, when $M_{\text{disk}} = 21 M_{\oplus}$. Here we adopted the disruption law for ice from Benz & Asphaug (1999) and $f_Q = 0.1$. The red line shows the size distribution of known Jupiter Trojans (incomplete for $D < 10$ km) scaled up by their implantation efficiency (Nesvorný et al. 2013). Panel (b): collisional survival of equal-size binaries in the disk. The lines show the results for $t_{\text{disk}} = 10$ Myr and $R_1 + R_2 = 30, 100$ and 300 km.

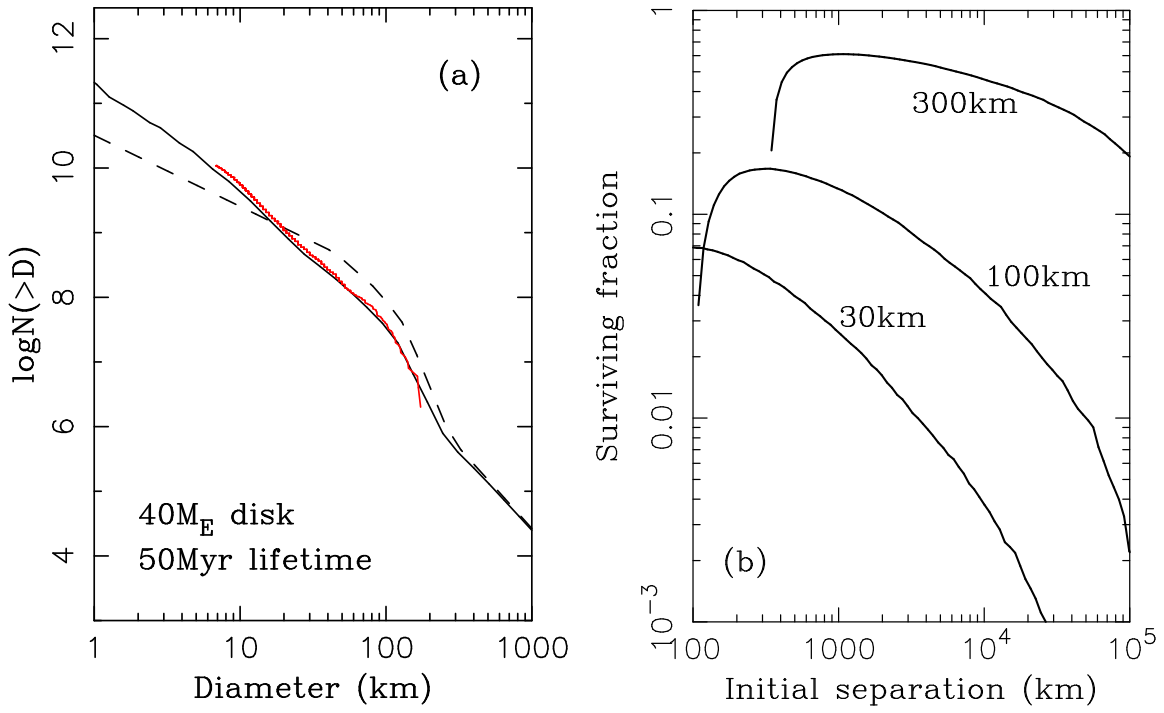


Fig. 10.— The same as Fig. 9 but for $M_{\text{disk}} = 40 M_{\oplus}$, $t_{\text{disk}} = 50 \text{ Myr}$ and $f_Q = 0.3$.

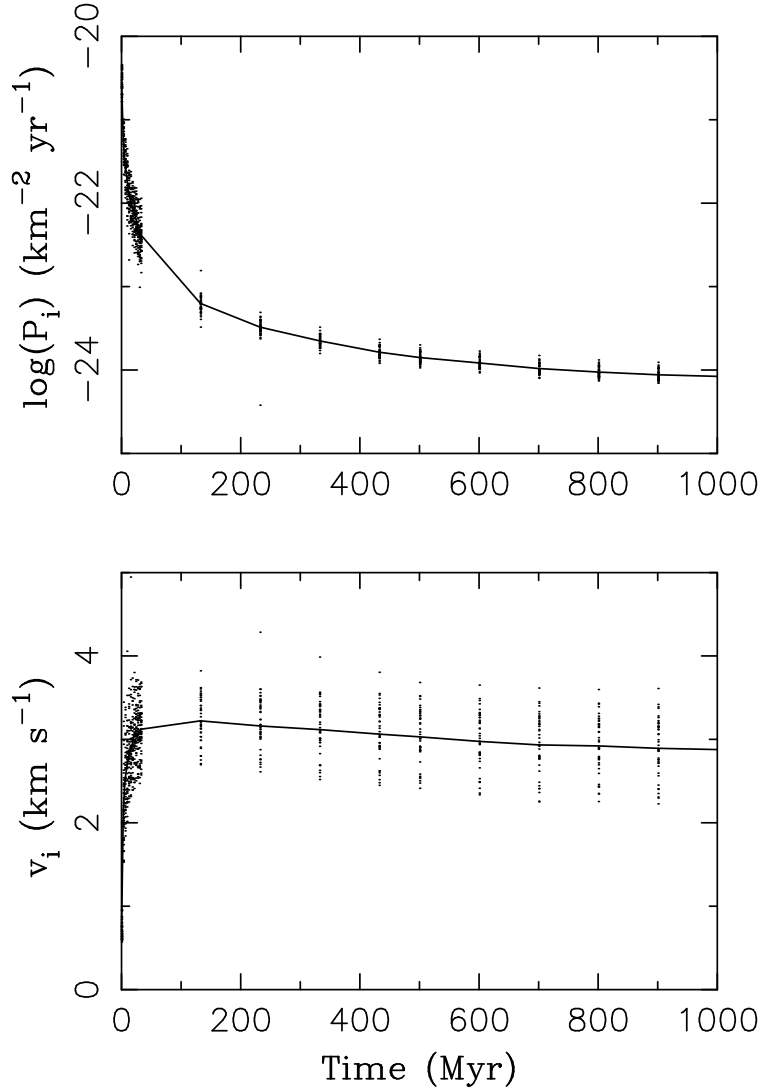


Fig. 11.— The collision probability (P_i) and impact speed (v_i) of planetesimals. $P_i(t)$ was normalized by the *initial* number of planetesimals. Its value at any given time therefore encapsulates both the changing collision probability and decaying population of planetesimals. Here we assumed that the disk was dispersed by migrating Neptune immediately after t_0 . Time $t = 0$ in this plot therefore corresponds to the onset of Neptune’s migration into the outer planetesimal disk. At $t = 0$, $P_i = 4 \times 10^{-21} \text{ km}^{-2} \text{ yr}^{-1}$ and $v_i = 0.6 \text{ km}$, which is in the ballpark of the values considered for the simulations in Section 5.3. The normalized probability drops over time as the disk planetesimals are dispersed and eliminated from the solar system. Here, $P_i(t)$ and $v_i(t)$ are shown for the case2 migration parameters and HCs. The results for case1 and other KBO categories are similar.

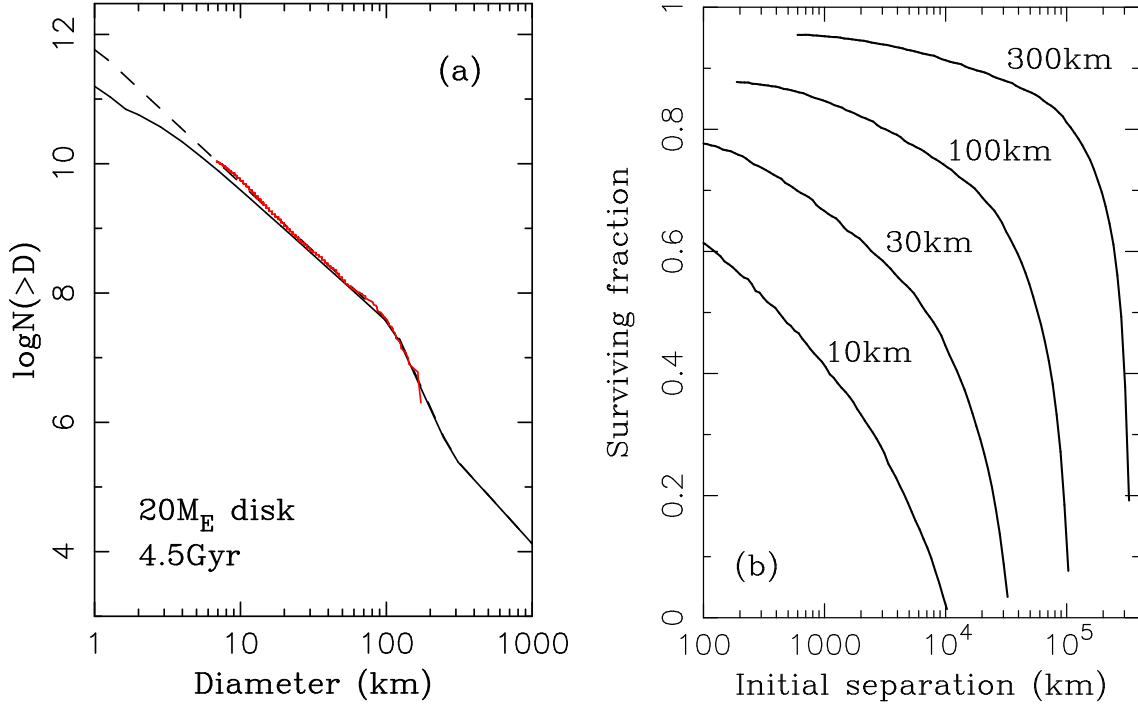


Fig. 12.— The *Boulder* code results for $t_{\text{disk}} = 0$. In panel (a), we assumed that $M_{\text{disk}} = 20 M_{\oplus}$ at $t = 0$ and the initial size distribution (solid line) similar to that of Jupiter Trojans (solid red line). The size distribution does not change much over time and the final distribution ($t = 4.5$ Gyr; solid black line) is similar to the initial one. In panel (b), the survival probability is shown for the equal-size binaries with $R_1 + R_2 = 10, 30, 100$ and 300 km (as labeled). These results were obtained for $P_1(t)$ and $v_i(t)$ shown in Figure 11.

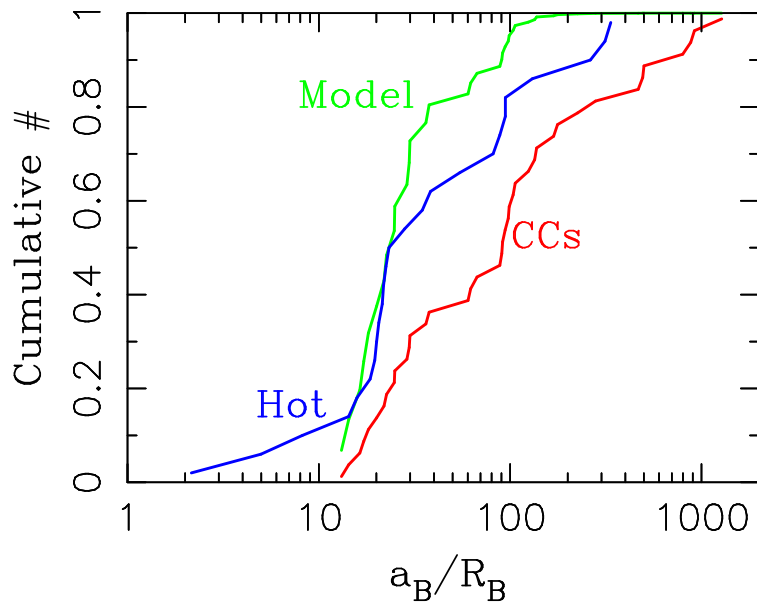


Fig. 13.— The cumulative distribution of known equal-size ($R_2/R_1 > 0.5$) binaries in the dynamically cold (red line) and hot populations (blue line). The model distribution (green line) was obtained by applying the dynamical survival probability from Fig. 3 to a template distribution (see the main text).